Master Thesis

Doubly-Selective Channel Estimation for LTE-A Uplink

at the Institute of Telecommunications,
TU Wien

Author
Stefan Pratschner, BSc

Matriculation Number
1025842

Advisor
Univ.Prof. Dipl.-Ing. Dr.techn. Markus Rupp

Co-Advisor
Univ.Ass. Dipl.-Ing. Dr.techn. Stefan Schwarz

Vienna, May 20, 2016

TECHNISCHE UNIVERSITÄT WIEN
Vienna | Austria

institute of telecommunications

Abstract

Today the most recent standard for mobile communications is known as LTE-Advanced (LTE-A), developed and organized by the 3rd Generation Partnership Project. As a 4th generation system for mobile communication, LTE-A offers high flexibility in terms of deployment aspects and resource allocation as well as high spectral efficiency. To achieve these main features, sophisticated link level access schemes, such as orthogonal frequency division multiplexing and Multiple-Input Multiple-Output (MIMO) technologies, are employed.

For such a wireless communication system, coherent detection at the receive side is essential to obtain intended overall performance. This requires knowledge of the wireless channel, making channel estimation not only necessary but a very important task within the signal processing chain.

In LTE-A reference symbols, which are known to the receiver, are multiplexed with the transmitted data to enable channel estimation. In uplink MIMO transmissions, these pilot symbols are multiplexed on the same time-frequency positions for all spatial layers, making separation of estimated MIMO channels necessary. Many existing estimation methods aim for separation in time domain, exploiting the reference symbols' code-domain orthogonality. These algorithms suffer from overlapping Channel Impulse Responses (CIR) when estimating frequency selective channels, referred to as CIR leakage.

In my work I present channel estimation algorithms that aim to separate all estimated MIMO channels in frequency domain. These methods do not suffer from CIR leakage and achieve a significantly lower estimation error when estimating frequency selective channels. Further, I introduce and compare several interpolation methods that enable to obtain channel coefficients in between pilot positions, making estimation of doubly selective MIMO channels possible. I compare and discuss performance of presented estimation methods in terms of mean square error and resulting bit error ratio as obtained by simulations, in the context of single-user and multi-user MIMO.

Kurzfassung

Der aktuellste Standard für mobile Kommunikation heutzutage ist als LTE-Advanced (LTE-A) bekannt, und wird vom 3rd Generation Partnership Project entwickelt und verwaltet. Als ein mobiles Kommunikationsystem der 4ten Generation bietet LTE-A hohe Flexibilität im Bezug auf Einsatzmöglichkeiten und Ressourcen Verteilung, so wie hohe spektrale Effizienz. Um diese Hauptmerkmale zu erreichen werden ausgereifte Zugriffsverfahren auf der physikalischen Netzwerkschicht, wie Orthogonal Frequency Division Multiplexing (OFDM) und Multiple-Input Multiple-Output (MIMO), verwendet. Für solche drahtlosen Kommunikationssysteme ist kohärente Detektion auf der Empfängerseite essentiell um die angestrebte Leistungsfähigkeit zu erreichen. Dies erfordert Kenntnis des Übertragungskanals, was Kanalschätzung nicht nur notwendig, sondern zu einer wichtigen Aufgabe innerhalb der Signalverarbeitungskette macht.

In LTE-A werden Referenzsymbole, welche dem Empfänger bekannt sind, mit den Daten kombiniert übertragen, um Kanalschätzung zu ermöglichen. Bei Uplink MIMO Übertragungen werden diese Referenzsymbole aller räumlichen Datenströme auf den gleichen Zeit-Frequenz Positionen übertragen, weswegen eine Separation der geschätzten MIMO Kanäle notwendig ist. Viele bekannte Schätzmethoden zielen auf eine Separation im Zeitbereich ab, bei welcher die Orthogonalität der Referenzsymbole im Code-Bereich genützt wird. Diese Algorithmen leiden unter der Überlappung der Kanalimpulsantworten bei der Schätzung von frequenzselektiven Kanälen.

In meiner Arbeit entwerfe ich Algorithmen zur Kanalschätzung, welche auf die Separation der MIMO Kanäle im Frequenzbereich abzielen. Diese Methoden leiden nicht unter der Überlappung der Kanalimpulsantworten und erzielen signifikant reduzierte Kanalschätzfehler bei der Schätzung von frequenzselektiven Kanälen. Weiters zeige und vergleiche ich verschiedene Interpolationsmethoden welche es ermöglichen Kanalkoeffizienten zwischen Referenzsymbol Positionen zu erlangen, um die Schätzung von Zeit-Frequenz selektiven Kanälen zu ermöglichen. Ich beschreibe und vergleiche die Leistungsfähigkeit der präsentierten Methoden zur Kanalschätzung anhand des mittleren quadratischen Kanalschätzfehlers und der resultierenden Bitfehlerrate durch Simulationen, sowohl für Single-User als auch Multi-User MIMO.

List of Acronyms

3GPP	3rd Generation Partnership Project
BER	Bit Error Ratio
BS	Base Station
CE	Channel Estimation
CIR	Channel Impulse Response
CLSM	Closed Loop Spatial Multiplexing
CP	Cyclic Prefix
CSF	Cyclic Shift Field
DCI	Downlink Control Information
DCT	Discrete Cosine Transform
DFT	Discrete Fourier Transform
DMRS	Demodulation Reference Signal
DPSS	Discrete Prolate Spheroidal Sequence
FD-CDM	Frequency Domain Code Division Multiplexing
ICI	Inter-Carrier Interference
IDFT	Inverse Discrete Fourier Transform
LMMSE	Linear MMSE
LS	Least Squares
LTE	Long Term Evolution
LTE-A	LTE-Advanced
LTI	Linear Time Invariant
MIMO	Multiple-Input Multiple-Output
MMSE	Minimum Mean Square Error

MSE	Mean Square Error
MU	Multi-User
MU-MIMO	Multi-User MIMO
OCC	Orthogonal Cover Code
OFDM	Orthogonal Frequency Division Multiplexing
PAPR	Peak-to-Average Power Ratio
PedA	Pedestrian A
PMI	Precoding Matrix Indicator
PUSCH	Physical Uplink Shared Channel
QAM	Quadrature Amplitude Modulation
QS	Quadratic Smoothing
RB	Resource Block
RE	Resource Element
RMS	Root Mean Square
SC-FDM	Single-Carrier Frequency Division Multiplexing
SISO	Single-Input Single-Output
SNR	Signal to Noise Ratio
SRS	Sounding Reference Signal
SU	Single-User
SU-MIMO	Single-User MIMO
TTI	Transmission Time Interval
TU	Typical Urban
UE	User Equipment
UMTS	Universal Mobile Telecommunication System
VehB	Vehicular B
ZC	Zadoff-Chu

Contents

1 Outlook and Contributions

In this work I consider the problem of estimating the wireless channel at the receive side of an LTE-Advanced (LTE-A) uplink Multiple-Input Multiple-Output (MIMO) transmission. Estimating all MIMO channels is especially challenging when the channel is time and frequency selective. I show that in this case, implications for channel estimation do not arise due to the Single-Carrier Frequency Division Multiplexing (SC-FDM) physical layer access scheme but mainly due to the specific allocation pattern of reference symbols in the LTE-A uplink. Within this thesis I introduce algorithms to estimate and interpolate the wireless channel for the purpose of demodulation, exploiting the special code-domain orthogonality of reference symbols.

In Section 2 and Section 3, a general introduction to the LTE-A uplink is given. In this context a system model in vector notation, capable of describing Single-User MIMO (SU-MIMO) SC-FDM transmissions, is derived. These chapters mainly rely on our work in [1].

The unique properties of reference signals in the LTE-A uplink are explained in Section 4. Based on my contributions in [2], their specific allocation scheme and the implications for channel estimation are presented. The code-domain structure of reference symbols introduced in this section is heavily exploited throughout my thesis.

Based on my work in [3], novel methods for channel estimation that operate entirely in frequency domain are introduced in Section 5. These algorithms show superior capability of separating estimated MIMO channels, leading to lower estimation errors compared to well-known Discrete Fourier Transform (DFT) based estimation methods.

In Section 6, a system model for Multi-User MIMO (MU-MIMO) transmissions that is derived from the Single-User (SU) system model in a straight forward manner is presented, as done in our work [4]. As it is possible to obtain code-domain orthogonality between users by means of signaling, estimation methods derived for SU-MIMO are also applicable in the MU-MIMO case.

To obtain channel coefficients in between pilot positions and to enable doubly-selective channel estimation, various channel interpolation methods are discussed and compared in Section 7. Storing and considering estimated channel coefficients from previous subframes significantly improves channel estimation under certain circumstances, as we also considered in our work in [1].

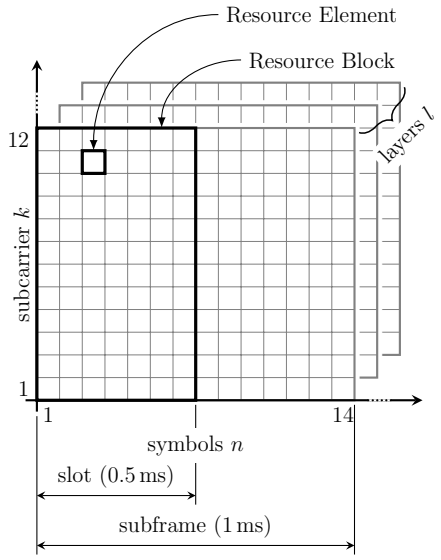

Figure 1: Illustration of the LTE-A resource grid for multiple spatial layers.

2 Introduction to the LTE-A Uplink

The 3rd Generation Partnership Project (3GPP) Universal Mobile Telecommunication System (UMTS) successor, UMTS Long Term Evolution (LTE), was introduced in 2008 (3GPP Rel.8), offering data rates of up to 300 Mbit/s in the downlink and 75 MBit/s in the uplink. High spectral efficiency was reached by employing Orthogonal Frequency Division Multiplexing (OFDM) as the physical layer access scheme and by allowing for 4×4 MIMO transmissions in the downlink. However, the first release meeting 3GPP's requirements for 4^{th} generation mobile communication systems [5] was 3GPP Rel. 10 in 2011, namely LTE-A. Since then, MIMO transmissions are possible in the LTE-A uplink as well.

While OFDM is employed in LTE-A as physical layer access scheme for downlink, SC-FDM is employed for uplink in order to achieve a low Peak-to-Average Power Ratio (PAPR). In both cases, radio resources are organized in a time-frequency grid, as shown in Fig. 1. Here the frequency is given in OFDM subcarriers k while time scaling is given in OFDM symbol indices n. A single time-frequency grid position is referred to as Resource Element (RE), containing one modulated symbol. In 3GPP LTE, resources are partitioned into frames within time domain. A radioframe with a duration of 10 ms

consists of 10 subframes, each of 1 ms length.[1] A subframe, which is exactly one Transmission Time Interval (TTI), is further split into two slots of 0.5 ms each, as illustrated in Fig. 1. In case of normal Cyclic Prefix (CP) length, each slot contains 7 OFDM symbols, while it contains only 6 OFDM symbols if an extended CP length is employed. REs are clustered into so called Resource Block (RB)s with a time duration of one slot and a frequency span of 12 subcarriers. Given a 15 kHz OFDM subcarrier spacing[2], a RB therefore comprises 180 kHz in frequency domain and 0.5 ms in time domain. It is the smallest unit of resources in terms of user allocation.

For a mobile communication system such as LTE-A, channel estimation is a crucial factor for overall system performance. At the receive side, equalization and detection is carried out, based on the estimated channel. The quality of Channel Estimation (CE) therefore directly influences the Bit Error Ratio (BER) and rate of data transmission. For the purpose of CE, pilot symbols, or reference signals, are employed in LTE-A. By inserting these known symbols at predefined positions in the time-frequency resource grid at the transmit side, the channel can be estimated by the receiver. Pilot aided CE is a well established method for OFDM systems [6–9]. Estimation algorithms can be directly adopted for the LTE-A downlink, in the Single-Input Single-Output (SISO) as well as in the MIMO case. In the LTE-A uplink however, the allocation of reference symbols in case of MIMO transmissions prohibits direct application of OFDM CE methods. Due to the allocation of reference signals from different spatial layers on the same REs, the pilot symbols interfere with each other. In order to separate reference signals of different layers at the receiver, a special orthogonal reference symbol structure is employed in LTE-A [10–12]. Unfortunately, orthogonality is destroyed by transmission over a frequency selective channel.

The most common approach for channel estimation in the LTE uplink is DFT or Discrete Cosine Transform (DCT) based channel estimation [13–17] which is also known from OFDM systems [18]. For LTE-A, when Closed Loop Spatial Multiplexing (CLSM) is employed, these methods aim to separate the estimated Channel Impulse Response (CIR)s from all active spatial layers in time domain. For a frequency flat channel, the orthogonality of reference signals is preserved and channel estimation is similar to the SISO case [19]. However, when estimating frequency selective channels of multiple spatial layers in time domain, CIRs may overlap and cannot be separated any more, which is referred to as CIR leakage [20–22]. Therefore, much effort was put

[1] In this thesis I only consider the frequency division duplexing frame structure of LTE-A.

[2] In the LTE-A uplink, this is the only standardized subcarrier spacing whereas there is also a 7.5 kHz subcarrier spacing defined in the downlink.

into the improvement of DFT or DCT based CE methods [13, 15, 16, 23, 24]. Still, CIR leakage is inevitable when a user is assigned only a small portion of the uplink bandwidth and the wireless channel has a non negligible delay spread.

If not only a single user is transmitting, i.e. SU-MIMO, but several users are allocated the same resources, i.e. MU-MIMO, similar implications for CE apply [16, 20, 24–26]. In that case, reference signals on different spatial layers, originating from multiple users, overlap and need to be separated at the receiver. Therefore, transmissions over frequency selective channels again lead to CIR leakage in MU-MIMO transmissions, as in the SU-MIMO case.

When the channel is not only frequency selective but also time variant, i.e., doubly selective, CE is even more challenging. For a fast time-varying scenario, the channel coefficients of an OFDM system are no longer constant during the duration of an OFDM symbol, leading to Inter-Carrier Interference (ICI). In terms of channel estimation, these effects can be captured by the channel estimator, or ICI is mitigated after CE [7, 27, 28]. However, the occurring ICI is dominant only at very high speeds [29], making LTE-A robust in high mobility environments. Assuming the channel to be constant for the duration of an OFDM symbol as approximation, the estimated channel has to be interpolated in between pilot positions in order to obtain a complete channel estimate for the whole time-frequency grid.

In my thesis I first introduce a SU-MIMO SC-FDM system model in matrix notation in Section 3, capable of describing relations between subcarriers due to the DFT spreading of data and reference symbols. In Section 4 I describe the allocation and structure of employed reference symbols in the LTE-A uplink for CE. For the purpose of comparison I introduce DFT based CE and Minimum Mean Square Error (MMSE) estimation in the beginning of Section 5, which is followed by the main contribution of my work: two Least Squares (LS) based estimation methods. Based on the solution of an LS estimation problem, I derive two versions of CE by post-processing in frequency domain, leading to low complexity CE algorithms. Both of these methods show advantages over DFT based estimation, especially for a small transmission bandwidth. In Section 6 the introduced methods are generalized to the case of MU-MIMO transmissions, where challenges in CE are very similar to SU-MIMO transmissions. In order to obtain estimated channel coefficients also on data positions, I consider interpolation in time domain for time varying channels in Section 7. Finally, I compare performance of introduced estimation and interpolation methods in Section 8, where also conclusions and possibilities for future work are discussed.

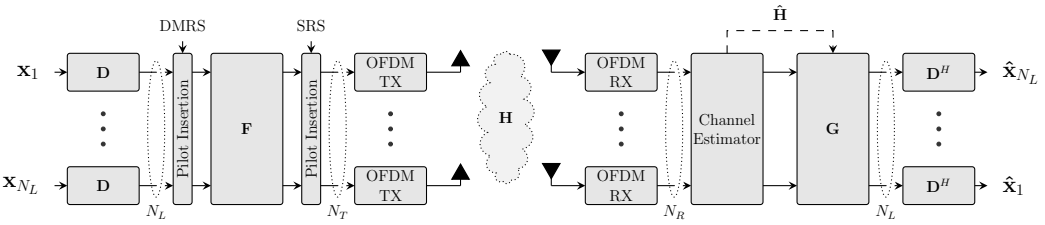

Figure 2: The LTE-A uplink MIMO system model.

3 Single-User-MIMO System Model

SC-FDM is DFT spread OFDM. This means, each transmit symbol is spread across all subcarriers by means of a layer-wise DFT, as illustrated in Fig. 2 by DFT matrix $\mathbf{D}$ on the very left, leading to the single-carrier like characteristic of this modulation method. Due to the OFDM processing, subcarriers are indeed orthogonal. However, DFT spreading is carried out across all subcarriers such that transmit signals on different subcarriers are not independent any more. A system model on subcarrier basis, as it is often seen for MIMO OFDM systems, is not the method of choice to describe such a system. Instead, for a SC-FDM model, all subcarriers k at one symbol time n are represented in vector notation as in [30]. In terms of a MIMO system model, these vectors will be stacked to describe an SC-FDM system for each spatial transmission layer or receive antenna. This leads to a linear system description exploiting block-wise Toeplitz, circulant and diagonal structured matrices as done in [31, 32]. To reveal this structure, the system model is introduced in an inside-out fashion, starting with the convolution of the transmit signal with the CIR.

Assuming the channel to be constant in time, for the duration of one OFDM symbol with symbol time index n, convolution of the transmit signal with the discrete CIR $\mathbf{h}_{n,r,t} \in \mathbb{C}^{N_h \times 1}$ from transmit antenna t to receive antenna r is denoted by multiplication with Toeplitz matrix $\mathbf{H}^{(\text{toep})}_{n,r,t} \in$

$\mathbb{C}^{(N_{\mathrm{FFT}}+N_{\mathrm{CP}})\times(N_{\mathrm{FFT}}+N_{\mathrm{CP}})}$ defined by

$$\mathbf{H}_{n,r,t}^{(\mathrm{toep})} = \begin{pmatrix} \mathbf{h}_{n,r,t}[1] & & & & & & & \\ \mathbf{h}_{n,r,t}[2] & \mathbf{h}_{n,r,t}[1] & & & & & & \\ \vdots & \mathbf{h}_{n,r,t}[2] & \ddots & & & & & \\ \mathbf{h}_{n,r,t}[N_h] & \vdots & \ddots & \ddots & & & & \\ & \mathbf{h}_{n,r,t}[N_h] & & \ddots & \ddots & & & \\ & & \ddots & & \ddots & \ddots & & \\ & & & \mathbf{h}_{n,r,t}[N_h] & \dots & \mathbf{h}_{n,r,t}[2] & \mathbf{h}_{n,r,t}[1] \end{pmatrix}, \tag{3.1}$$

where square brackets denote vector entries. In order to describe a MIMO system, with N_T transmit and N_R receive antennas, this matrix is then stacked to obtain a block-wise Toeplitz matrix

$$\mathbf{H}_{n}^{(\mathrm{toep})} = \begin{pmatrix} \mathbf{H}_{n,1,1}^{(\mathrm{toep})} & \dots & \mathbf{H}_{n,1,N_T}^{(\mathrm{toep})} \\ \vdots & \ddots & \vdots \\ \mathbf{H}_{n,N_R,1}^{(\mathrm{toep})} & \dots & \mathbf{H}_{n,N_R,N_T}^{(\mathrm{toep})} \end{pmatrix} \in \mathbb{C}^{(N_{\mathrm{FFT}}+N_{\mathrm{CP}})N_R\times(N_{\mathrm{FFT}}+N_{\mathrm{CP}})N_T}. \tag{3.2}$$

Exploiting this block-wise Toeplitz structured matrix for convolution describes the channel as Linear Time Invariant (LTI) system within each OFDM symbol period.

Further assuming the CP length to be at least the CIR length, i.e., $N_{\mathrm{CP}} \geq N_h$, this Toeplitz matrix is first block-wise circularized by adding and removing the CP, represented by

$$\mathbf{P}_{\mathrm{addCP}} = \begin{pmatrix} \mathbf{0} & \mathbf{I}_{N_{\mathrm{CP}}} \\ & \mathbf{I}_{N_{\mathrm{FFT}}} \end{pmatrix} \in \mathbb{R}^{(N_{\mathrm{FFT}}+N_{\mathrm{CP}})\times N_{\mathrm{FFT}}}, \tag{3.3}$$

and

$$\mathbf{P}_{\mathrm{remCP}} = \begin{pmatrix} \mathbf{0} & \mathbf{I}_{N_{\mathrm{FFT}}} \end{pmatrix} \in \mathbb{R}^{N_{\mathrm{FFT}}\times(N_{\mathrm{FFT}}+N_{\mathrm{CP}})}, \tag{3.4}$$

respectively, leading to [3]

$$\mathbf{H}_{n}^{(\mathrm{circ})} = (\mathbf{I}_{N_R} \otimes \mathbf{P}_{\mathrm{remCP}})\, \mathbf{H}_{n}^{(\mathrm{toep})}\, (\mathbf{I}_{N_T} \otimes \mathbf{P}_{\mathrm{addCP}}) \in \mathbb{C}^{N_{\mathrm{FFT}}N_R\times N_{\mathrm{FFT}}N_T}. \tag{3.5}$$

Further, applying a DFT of size N_{FFT}, represented by matrix $\mathbf{D}_{N_{\mathrm{FFT}}}$, and an Inverse Discrete Fourier Transform (IDFT), the channel matrix is

[3] Please note, that in the case of insufficient CP length, the block-wise Toeplitz matrix $\mathbf{H}^{(\mathrm{toep})}$ will not get circularized. The matrix $\mathbf{H}^{(\mathrm{circ})}$ will therefore not have a block-wise circulant structure and as a consequence, $\mathbf{H}^{(\mathrm{diag})}$ will not have a block-wise diagonal structure [32].

block-wise diagonalized, yielding

$$\mathbf{H}_n^{(\mathrm{diag})} = \left(\mathbf{I}_{N_R} \otimes \mathbf{D}_{N_{\mathrm{FFT}}}\right) \mathbf{H}_n^{(\mathrm{cir})} \left(\mathbf{I}_{N_T} \otimes \mathbf{D}_{N_{\mathrm{FFT}}}^H\right) \in \mathbb{C}^{N_{\mathrm{FFT}}N_R \times N_{\mathrm{FFT}}N_T} \ . \quad (3.6)$$

The block-wise diagonal channel matrix $\mathbf{H}_n^{(\mathrm{diag})} \in \mathbb{C}^{N_{\mathrm{FFT}}N_R \times N_{\mathrm{FFT}}N_T}$ is a matrix of channel coefficients for each subcarrier. Still assuming sufficient CP length, this matrix is constructed by applying DFTs on the CIRs

$$\mathbf{H}_n^{(\mathrm{diag})} = \begin{pmatrix} \mathrm{Diag}\left(\mathbf{D}_{N_{\mathrm{FFT}}} \bar{\mathbf{h}}_{n,1,1}\right) & \dots & \mathrm{Diag}\left(\mathbf{D}_{N_{\mathrm{FFT}}} \bar{\mathbf{h}}_{n,1,N_T}\right) \\ \vdots & \ddots & \vdots \\ \mathrm{Diag}\left(\mathbf{D}_{N_{\mathrm{FFT}}} \bar{\mathbf{h}}_{n,N_R,1}\right) & \dots & \mathrm{Diag}\left(\mathbf{D}_{N_{\mathrm{FFT}}} \bar{\mathbf{h}}_{n,N_R,N_T}\right) \end{pmatrix} \quad (3.7)$$

with the zero padded time domain CIR vector $\bar{\mathbf{h}}_{n,r,t} = \left(\mathbf{h}_{n,r,t}^T, 0, \dots, 0\right)^T \in \mathbb{C}^{N_{\mathrm{FFT}} \times 1}$, as explained in Appendix A.1.

Including the localized subcarrier mapping, described by[4]

$$\mathbf{M} = \begin{pmatrix} \mathbf{0} \\ \mathbf{I}_{N_{\mathrm{SC}}} \\ \mathbf{0} \end{pmatrix} \in \mathbb{R}^{N_{\mathrm{FFT}} \times N_{\mathrm{SC}}} \ , \quad (3.8)$$

finally the effective channel matrix is obtained as

$$\mathbf{H}_n = \left(\mathbf{I}_{N_R} \otimes \mathbf{M}^H\right) \mathbf{H}_n^{(\mathrm{diag})} \left(\mathbf{I}_{N_T} \otimes \mathbf{M}\right) \left(\mathbf{F}_n \otimes \mathbf{I}_{N_{\mathrm{SC}}}\right) \in \mathbb{C}^{N_{\mathrm{SC}}N_R \times N_{\mathrm{SC}}N_L} \ , \quad (3.9)$$

with precoding matrix $\mathbf{F} \in \mathbb{C}^{N_T \times N_L}$ according to the LTE-A codebook [10]. To obtain the same transmit power for any number of employed spatial layers N_L, the precoder is normalized such that it's squared Frobenius norm is one, i.e., $\mathrm{trace}\{\mathbf{F}^H\mathbf{F}\} = 1$.

The OFDM signal processing, meaning the IDFT and DFT transform, CP addition and removal and the localized subcarrier mapping and demapping, is shown by the blocks *OFDM TX* and *OFDM RX* in Fig. 2 at the transmitter and receiver, respectively.

Transmit symbols of layer $l \in \{1, \dots, N_L\}$ at OFDM symbol time n of all N_{SC} subcarriers are described by vector $\mathbf{x}_{n,l} \in \mathcal{A}^{N_{\mathrm{SC}} \times 1}$ with symbol alphabet $\mathcal{A}$. Data symbols are assumed to be of power P_x and statistically independent, i.e., $\mathbb{E}\{\mathbf{x}_{n,l}\mathbf{x}_{n,l}^H\} = P_x\mathbf{I}_{N_{\mathrm{SC}}}$. In terms of the full MIMO SC-FDM system model, the transmit symbols $\mathbf{x}_{n,l}$ of all spatial layers $l \in \{1, \dots, N_L\}$ are stacked in a similar way as the MIMO channel matrices to obtain

$$\mathbf{x}_n = \begin{pmatrix} \mathbf{x}_{n,1} \\ \mathbf{x}_{n,2} \\ \vdots \\ \mathbf{x}_{n,N_L} \end{pmatrix} \in \mathcal{A}^{N_{\mathrm{SC}}N_L \times 1} \ . \quad (3.10)$$

[4]This subcarrier mapping implicitly assumes a single user that is scheduled on all N_{SC} available subcarriers.

Exploiting this symbol vector and introducing the linear receiver $\mathbf{G} \in \mathbb{C}^{N_{\mathrm{SC}}N_L \times N_{\mathrm{SC}}N_R}$, the symbol estimates on the receiver side $\hat{\mathbf{x}}_n \in \mathbb{C}^{N_{\mathrm{SC}}N_L \times 1}$ are given by[5]

$$\begin{aligned}\hat{\mathbf{x}}_n &= \left(\mathbf{I}_{N_L} \otimes \mathbf{D}_{N_{\mathrm{SC}}}^H\right) \mathbf{G}_n \mathbf{H}_n \left(\mathbf{I}_{N_L} \otimes \mathbf{D}_{N_{\mathrm{SC}}}\right) \mathbf{x}_n \\ &\quad + \left(\mathbf{I}_{N_L} \otimes \mathbf{D}_{N_{\mathrm{SC}}}^H\right) \mathbf{G}_n \underbrace{\left(\mathbf{I}_{N_R} \otimes \mathbf{M}^H \mathbf{D}_{N_{\mathrm{FFT}}} \mathbf{P}_{\mathrm{remCP}}\right) \tilde{\mathbf{z}}_n}_{\mathbf{z}_n} \\ &= \left(\mathbf{I}_{N_L} \otimes \mathbf{D}_{N_{\mathrm{SC}}}^H\right) \mathbf{G}_n \mathbf{H}_n \left(\mathbf{I}_{N_L} \otimes \mathbf{D}_{N_{\mathrm{SC}}}\right) \mathbf{x}_n + \left(\mathbf{I}_{N_L} \otimes \mathbf{D}_{N_{\mathrm{SC}}}^H\right) \mathbf{G}_n \mathbf{z}_n \ , \quad (3.11)\end{aligned}$$

with the independent and identically distributed white Gaussian noise vector $\tilde{\mathbf{z}}_n \sim \mathcal{CN}(\mathbf{0}, \sigma_{\mathbf{z}}^2 \mathbf{I}_{(N_{\mathrm{FFT}}+N_{\mathrm{CP}})N_R})$.

[5] Please note, that within this context, substituting the DFT spreading and de-spreading by the identity function, a MIMO OFDM model would be obtained, i.e., $\hat{\mathbf{x}}_n = \mathbf{G}_n \mathbf{H}_n \mathbf{x}_n + \mathbf{G}_n \mathbf{z}_n$.

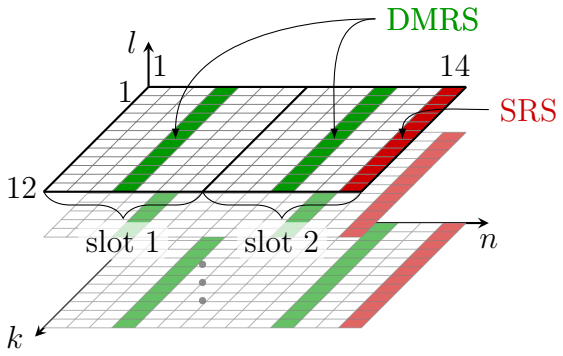

Figure 3: The LTE-A uplink reference symbol allocation in two slots (one subframe).

4 Reference Symbols

In LTE-A, CE is pilot aided. For this reason, reference signals are multiplexed with data at certain positions of the resource grid. Based on the knowledge of pilot symbols, channel coefficients can be estimated at pilot positions at the receiver side. In order to obtain channel estimates on data positions, the estimated channel is then interpolated in between pilot positions.

There are two different types of reference signals defined in the LTE-A uplink, namely Demodulation Reference Signal (DMRS) and Sounding Reference Signal (SRS). DMRS are employed for CE for the purpose of coherent detection and span the whole user assigned bandwidth in a Physical Uplink Shared Channel (PUSCH) transmission. SRS are transmitted on the whole available uplink bandwidth for the purpose of channel sounding. Channel estimates obtained from SRS are utilized for calculation of link adaptation parameters, such as Precoding Matrix Indicator (PMI), and scheduling [33]. To enable precoder selection based on SRS CE, these reference signals are inserted after the precoder, as shown in Fig. 2, meaning there is one SRS for each transmit antenna. DMRS on the other hand, are inserted before the precoder, meaning there is one DMRS per spatial layer, to enable for estimation of the effective channel.

The reference symbols are defined in [10] and are explained in more detail in [11, 12, 23]. As shown in Fig. 3, DMRS are multiplexed in the resource grid at OFDM symbol times $n = \{4, 11\}$ for normal CP length, and at symbol times $n = \{3, 10\}$ for extended CP length.[6] In a PUSCH transmission of the

[6]I will implicitly assume normal CP length in the remainder of this work since all methods adapt in a straight forward manner to the case of extended CP length.

Table 1: Dependence of $n^{(2)}_{\mathrm{DMRS},l}$ and the OCC $\mathbf{w}_l$ on the cyclic shift field.

Cyclic Shift Field	$n^{(2)}_{\mathrm{DMRS},l}$				$\mathbf{w}_l^T$			
	l=1	l=2	l=3	l=4	l=1	l=2	l=3	l=4
000	0	6	3	9	(1 1)	(1 1)	(1 -1)	(1 -1)
001	6	0	9	3	(1 -1)	(1 -1)	(1 1)	(1 1)
010	3	9	6	0	(1 -1)	(1 -1)	(1 1)	(1 1)
011	4	10	7	1	(1 1)	(1 1)	(1 1)	(1 1)
100	2	8	5	11	(1 1)	(1 1)	(1 1)	(1 1)
101	8	2	11	5	(1 -1)	(1 -1)	(1 -1)	(1 -1)
110	10	4	1	7	(1 -1)	(1 -1)	(1 -1)	(1 -1)
111	9	3	0	6	(1 1)	(1 1)	(1 -1)	(1 -1)

LTE-A uplink, a DMRS occupies all scheduled subcarriers. While this specific multiplexing scheme of reference symbols for uplink transmissions was chosen in order to achieve a low PAPR [34], reference symbols are allocated on the same resources for all spatial layers, meaning they are completely overlapping in the time-frequency grid, in order to save transmission overhead. In LTE-A, DMRS of different transmission layers in the same slot are therefore orthogonal in terms of Frequency Domain Code Division Multiplexing (FD-CDM) [11], to make them separable at the receiver. This is obtained by a cyclic shift of a base sequence. A DMRS therefore consists of a base sequence and a layer dependent cyclic shift.

The base sequence of a DMRS on N_{SC} subcarriers for one slot is denoted by $\bar{\mathbf{r}} \in \mathbb{C}^{N_{\mathrm{SC}} \times 1}$. I assume the user is assigned N_{SC} subcarriers starting at 1, i.e., $k \in \{1, 2, \ldots, N_{\mathrm{SC}}\}$. For $N_{\mathrm{SC}} \geq 36$ the base sequence is given by a Zadoff-Chu (ZC) sequence, while it is a computer generated constant amplitude zero autocorrelation sequence for $N_{\mathrm{SC}} < 36$ [11]. In either case, the base sequence $\bar{\mathbf{r}}$ is a complex exponential sequence, lying on the unit circle and therefore fulfils

$$|\bar{\mathbf{r}}[k]| = 1 \qquad \forall k \in \{1, \ldots, N_{\mathrm{SC}}\} \; . \tag{4.1}$$

Further, the base sequence depends on cell specific group and sequence indices to reduce inter-cell interference in multi-cell scenarios. The group and sequence indices are not indicated in (4.1) since only a single cell is considered in this work.

Similar to [26], a DMRS on layer l for one slot is given by[7]

$$\mathbf{R}_l = \mathrm{Diag}\left(\mathbf{r}_l\right) = \mathbf{T}_l \,\mathrm{Diag}\left(\bar{\mathbf{r}}\right) \,, \tag{4.2}$$

with the cyclic shift operator

$$\mathbf{T}_l = \mathrm{Diag}\left(e^{j0}, \ldots, e^{j\alpha_l(k-1)}, \ldots, e^{j\alpha_l(N_{\mathrm{SC}}-1)}\right) \,, \tag{4.3}$$

where the operator $\mathrm{Diag}(\cdot)$ yields a diagonal matrix from a vector. The layer dependent cyclic shift α_l is defined by

$$\alpha_l = \frac{2\pi n_{\mathrm{cs},l}}{12} \tag{4.4}$$

with

$$n_{\mathrm{cs},l} = \left(n^{(1)}_{\mathrm{DMRS}} + n^{(2)}_{\mathrm{DMRS},l} + n_{\mathrm{PN}}\right) \bmod 12 \,. \tag{4.5}$$

Parameter $n^{(1)}_{\mathrm{DMRS}}$ is given by higher layers and n_{PN} a cell specific pseudo-random sequence. The only layer dependent term in (4.5) is $n^{(2)}_{\mathrm{DMRS},l}$. This value is signalled in terms of the uplink related Downlink Control Information (DCI) format, in which a field of three bits is reserved for this purpose, namely the Cyclic Shift Field (CSF) [10, 34]. The relation between this CSF from DCI signalling and $n^{(2)}_{\mathrm{DMRS},l}$ is given by Table 1 which originates from Table 5.5.2.1.1-1 in [10]. Although this implies a dependence of DMRS on the CSF, this dependence is not considered until Section 6 as it does not affect any of the proposed schemes for SU-MIMO.

Since (4.5) leads to values $n^{(1)}_{\mathrm{DMRS}} \in \{0, 1, \ldots, 11\}$, (4.4) yields $\alpha_l \in \{0, \frac{2\pi}{12}, \ldots, 11\frac{2\pi}{12}\}$. Choosing the cyclic shift to be a multiple of $\frac{2\pi}{12}$ corresponds to the minimum number of 12 subcarriers assigned to a user. Therefore frequency domain orthogonality can be ensured even if a User Equipment (UE) is scheduled only a single RB.

As I will explain in Section 5, the inner product of two DMRS is the factor, determining the inter-layer interference. It is therefore crucial to analyse how the FD-CDM orthogonality can be exploited in order to cancel this interference. Exploiting (4.1), the product of two DMRS from layers l and p with $l, p \in \{1, \ldots, N_L\}$, becomes

$$\begin{aligned}\mathbf{R}_l^H \mathbf{R}_p =& \mathbf{T}_l^H \mathbf{T}_p \,\mathrm{Diag}\left(\bar{\mathbf{r}}\right)^H \mathrm{Diag}\left(\bar{\mathbf{r}}\right) \\ =& \,\mathrm{Diag}\left(e^{j0} \;\ldots\; e^{j\Delta\alpha_{l,p}(k-1)} \;\ldots\; e^{j\Delta\alpha_{l,p}(N_{\mathrm{SC}}-1)}\right) \mathbf{I} \,,\end{aligned} \tag{4.6}$$

[7]Please note, that the concept of OCC [10] is not introduced here since it does not affect the CE methods described in the following. Definition of DMRS will be augmented by OCC in Section 6.

with $\Delta\alpha_{l,p} = \alpha_p - \alpha_l$ being the cyclic phase shift between DMRS of two different spatial layers. The FD-CDM orthogonality can therefore be exploited as

$$\text{trace}\left(\mathbf{R}_p^H \mathbf{R}_l\right) = \mathbf{r}_p^H \mathbf{r}_l = \begin{cases} N_{\text{SC}} & \text{for } p = l \\ 0 & \text{for } p \neq l \end{cases}, \tag{4.7}$$

which implies that $\mathbf{R}_l$ is a unitary matrix, i.e., $\mathbf{R}_l^H = \mathbf{R}_l^{-1}$. After transmission over a frequency selective channel, this orthogonality has to be exploited to separate all effective MIMO channels at the receiver.

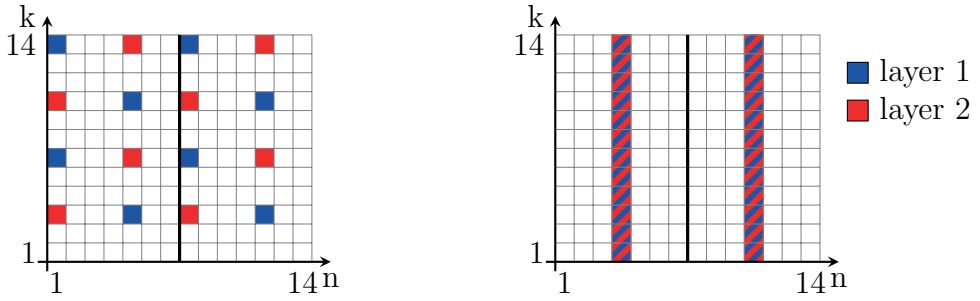

(a) The LTE-A downlink reference symbol allocation.

(b) The LTE-A uplink reference symbol allocation.

Figure 4: Comparison of DMRS allocation in LTE-A for two spatial layers.

5 Channel Estimation

In this section I consider CE for coherent detection based on DMRS. Since these reference signals are inserted prior to precoding, cf. Fig. 2, the effective channel (3.9) (including the precoder) is estimated. Also, the reference symbols are not DFT spreaded at the transmitter, and CE is carried out way before despreading at the receiver. The actual single carrier characteristic of SC-FDM does therefore not apply for CE. The main difference to CE in the LTE-A downlink, or to any other MIMO OFDM system, is the specific allocation of pilot symbols and their structure, as shown in Fig. 4. In the uplink, DMRS are multiplexed on the same resources for all active spatial layers in order to reduce overhead for uplink MIMO transmissions and to reduce the PAPR. Therefore they interfere with each other when being transmitted over a MIMO channel.[8] Exploiting the frequency domain orthogonality, the reference signals then have to be separated at the receiver in order to obtain channel estimates for all MIMO channels. Unfortunately this orthogonality is generally destroyed by a multipath channel and sophisticated estimation algorithms have to be applied. In this context it is obvious, that the problem of inter-layer interference is only present for transmission over a frequency selective MIMO channel. This complication neither arises on a frequency flat MIMO channel, as in [19], nor for SISO transmissions on a frequency selective channel [14]. Further, this effect is unique for uplink transmissions, since pilot symbols are multiplexed on distinct REs in the downlink, as shown in Fig. 4a.

[8]Due to the standardized precoder codebook [10], the inter-layer interference is actually caused by the MIMO channel rather than by the precoder, since there is only one data stream transmitted per transmit antenna.

5.1 System Model for Channel Estimation

As shown in Fig. 2, the DMRS are inserted after the DFT spreading, right before the precoding. As CE takes place right before the equalizer, the system model for CE reduces to an OFDM model, as there is no DFT spreading or de-spreading involved. The original model (3.11) therefore simplifies and the signal received at the channel estimator is

$$\mathbf{y}_n = \mathbf{H}_n \mathbf{r}_n + \mathbf{z}_n \ , \tag{5.1}$$

where the data $\mathbf{x}_n$ was substituted by the reference symbol $\mathbf{r}_n$. As explained in Section 4, DMRS are multiplexed at OFDM symbol times $n = \{4, 11\}$ in case of normal CP length. As (5.1) is therefore only exploited at these symbol times indices, the time index n will be omitted in the remainder of this section.

In order to reveal the stacked structure, (5.1) is expanded to

$$\begin{pmatrix} \mathbf{y}_1 \\ \vdots \\ \mathbf{y}_{N_R} \end{pmatrix} = \begin{pmatrix} \mathbf{H}_{1,1} & \dots & \mathbf{H}_{1,N_L} \\ \vdots & \ddots & \vdots \\ \mathbf{H}_{N_R,1} & \dots & \mathbf{H}_{N_R,N_L} \end{pmatrix} \begin{pmatrix} \mathbf{r}_1 \\ \vdots \\ \mathbf{r}_{N_L} \end{pmatrix} + \begin{pmatrix} \mathbf{z}_1 \\ \vdots \\ \mathbf{z}_{N_R} \end{pmatrix} \ . \tag{5.2}$$

Considering one row of this stacked model, the received signal on antenna i reads as

$$\begin{aligned} \mathbf{y}_i &= (\mathbf{H}_{i,1}, \dots, \mathbf{H}_{i,N_L}) \begin{pmatrix} \mathbf{r}_1 \\ \vdots \\ \mathbf{r}_{N_L} \end{pmatrix} + \mathbf{z}_i \\ &= (\mathbf{R}_1, \dots, \mathbf{R}_{N_L}) \begin{pmatrix} \mathbf{h}_{i,1} \\ \vdots \\ \mathbf{h}_{i,N_L} \end{pmatrix} + \mathbf{z}_i \ , \end{aligned} \tag{5.3}$$

where the block-wise diagonal structure of the effective channel matrix is exploited to form the channel vector $\mathbf{h}_{i,l} = \mathrm{diag}\,(\mathbf{H}_{i,l})$, where the operator $\mathrm{diag}(\cdot)$ yields a column vector from a matrix diagonal. Similarly the reference symbols are written as matrix $\mathbf{R}_l = \mathrm{Diag}\,(\mathbf{r}_l)$.

To perform channel estimation on this received signal in order to estimate the complete channel vector, (5.3) can be compactly written as

$$\mathbf{y}_i = \underline{\mathbf{R}}\underline{\mathbf{h}}_i + \mathbf{z}_i \ , \tag{5.4}$$

with

$$\underline{\mathbf{R}} = \big(\mathbf{R}_1 \dots \mathbf{R}_{N_L}\big) \in \mathbb{C}^{N_{\mathrm{SC}} \times N_{\mathrm{SC}} N_L} \ , \tag{5.5a}$$

$$\underline{\mathbf{h}}_i = \big(\mathbf{h}_{i,1}^T \dots \mathbf{h}_{i,N_L}^T\big)^T \in \mathbb{C}^{N_{\mathrm{SC}} N_L \times 1} \ . \tag{5.5b}$$

5.2 Minimum Mean Square Error Estimation

In this section a Linear MMSE (LMMSE) estimator is introduced. As it leads to the best performance in terms of Mean Square Error (MSE) among all linear estimators, it will serve as a lower bound on the CE MSE for all other estimation methods. To obtain this best estimator, the complete channel vector $\underline{\mathbf{h}}_i$ from (5.4) is estimated.

The LMMSE estimator $\mathbf{A} \in \mathbb{C}^{N_L N_{\mathrm{SC}} \times N_{\mathrm{SC}}}$ for estimating the channel vector $\hat{\underline{\mathbf{h}}}_i$ from the received signal as

$$\hat{\underline{\mathbf{h}}}_i = \mathbf{A}^{\mathrm{LMMSE}} \mathbf{y}_i \ , \tag{5.6}$$

is obtained by solving

$$\mathbf{A}^{\mathrm{LMMSE}} = \arg\min_{\mathbf{A}} \mathbb{E}\left\{ \left\| \mathbf{A}\mathbf{y}_i - \underline{\mathbf{h}}_i \right\|_2^2 \right\} \ . \tag{5.7}$$

As shown in Appendix A.2 the solution of this optimization problem is given by

$$\mathbf{A}^{\mathrm{LMMSE}} = \mathbf{C}_{\underline{\mathbf{h}}\mathbf{y}} \mathbf{C}_{\mathbf{y}}^{-1} \ , \tag{5.8}$$

with the correlation matrices $\mathbf{C}_{\underline{\mathbf{h}}\mathbf{y}} = \mathbb{E}\{\underline{\mathbf{h}}\mathbf{y}^H\}$ and $\mathbf{C}_{\mathbf{y}\mathbf{y}} = \mathbb{E}\{\mathbf{y}\mathbf{y}^H\}$. Inserting the system model (5.4) and assuming $\underline{\mathbf{h}}$ and $\mathbf{z}$ to be statistically independent, these correlations work out as

$$\begin{aligned} \mathbf{C}_{\mathbf{y}} =& \mathbb{E}\left\{\mathbf{y}\mathbf{y}^H\right\} \\ =& \mathbb{E}\left\{ \left(\underline{\mathbf{R}}\underline{\mathbf{h}} + \mathbf{z}\right) \left(\underline{\mathbf{R}}\underline{\mathbf{h}} + \mathbf{z}\right)^H \right\} \\ =& \underline{\mathbf{R}} \mathbf{C}_{\underline{\mathbf{h}}} \underline{\mathbf{R}}^H + \sigma_{\mathbf{z}}^2 \mathbf{I}_{N_{\mathrm{SC}}} \ , \end{aligned} \tag{5.9}$$

and

$$\begin{aligned} \mathbf{C}_{\underline{\mathbf{h}}\mathbf{y}} =& \mathbb{E}\left\{\underline{\mathbf{h}}\mathbf{y}^H\right\} \\ =& \mathbb{E}\left\{ \underline{\mathbf{h}} \left(\underline{\mathbf{R}}\underline{\mathbf{h}} + \mathbf{z}\right)^H \right\} \\ =& \mathbf{C}_{\underline{\mathbf{h}}} \underline{\mathbf{R}}^H \ . \end{aligned} \tag{5.10}$$

Inserting (5.9) and (5.10) into (5.8) yields the LMMSE estimator

$$\mathbf{A}^{\mathrm{LMMSE}} = \mathbf{C}_{\underline{\mathbf{h}}} \mathbf{R}^H \left(\underline{\mathbf{R}} \mathbf{C}_{\underline{\mathbf{h}}} \underline{\mathbf{R}}^H + \sigma_{\mathbf{z}}^2 \mathbf{I}_{N_{\mathrm{SC}}} \right)^{-1} \ . \tag{5.11}$$

Combining (5.6) and (5.11), the estimated channel is obtained by

$$\hat{\underline{\mathbf{h}}}_i^{\mathrm{LMMSE}} = \mathbf{C}_{\underline{\mathbf{h}}} \underline{\mathbf{R}}^H \left(\underline{\mathbf{R}} \mathbf{C}_{\underline{\mathbf{h}}} \underline{\mathbf{R}}^H + \sigma_{\mathbf{z}}^2 \mathbf{I}_{N_{\mathrm{SC}}} \right)^{-1} \mathbf{y}_i \ . \tag{5.12}$$

Inserting the expanded notation (5.5), the correlation matrix is

$$\mathbf{C}_{\underline{\mathbf{h}}} = \mathbb{E}\left\{ \begin{pmatrix} \mathbf{h}_{i,1} \\ \vdots \\ \mathbf{h}_{i,N_L} \end{pmatrix} \left(\mathbf{h}_{i,1}^H, \ldots, \mathbf{h}_{i,N_L}^H \right) \right\} . \tag{5.13}$$

Due to the stacking of channels from all layers into $\underline{\mathbf{h}}$ as described in (5.5), the correlation of $\underline{\mathbf{h}}$ can be written as

$$\mathbf{C}_{\underline{\mathbf{h}}} = \mathbf{C}_{\mathbf{h}}^{(s)} \otimes \mathbf{C}_{\mathbf{h}}^{(f)} , \tag{5.14}$$

with the channel frequency correlation matrix $\mathbf{C}_{\mathbf{h}}^{(f)} \in \mathbb{C}^{N_{\mathrm{SC}} \times N_{\mathrm{SC}}}$ and spatial correlation matrix $\mathbf{C}_{\mathbf{h}}^{(s)} \in \mathbb{C}^{N_L \times N_L}$.

The frequency correlation matrix describes the correlation between subcarriers and is given by

$$\mathbf{C}_{\mathbf{h}}^{(f)} = \mathop{\mathbb{E}}_{i,l}\{ \mathbf{h}_{i,l} \mathbf{h}_{i,l}^H \} . \tag{5.15}$$

The spatial correlation matrix describes the spatial correlation of the effective channel, this spatial correlation depends on the precoder $\mathbf{F} \in \mathbb{C}^{N_T \times N_L}$ as described in the following.[9] The stacked channel, including channel coefficients from N_{SC} subcarriers of all N_L layers to receive antenna i, $\underline{\mathbf{h}}_i \in \mathbb{C}^{N_{\mathrm{SC}} N_L \times 1}$ from (5.5) is an effective channel including the precoder. Considering (3.9) it can be written as

$$\underline{\mathbf{h}}_i = \left(\mathbf{F} \otimes \mathbf{I}_{N_{\mathrm{SC}}} \right)^T \underline{\mathbf{h}}'_i , \tag{5.16}$$

where $\underline{\mathbf{h}}'_i \in \mathbb{C}^{N_{\mathrm{SC}} N_T \times 1}$ denotes the channel without precoder and $\underline{\mathbf{h}}_i$ denotes the effective channel. Since the precoder $\mathbf{F}$ is constant over subcarriers k, (5.16) can be written on subcarrier basis as

$$[\underline{\mathbf{h}}_i]_k = \mathbf{F}^T [\underline{\mathbf{h}}'_i]_k , \tag{5.17}$$

where $[\cdot]_k$ selects the k^{th} subcarrier of the individual stacked vectors, as

$$[\underline{\mathbf{h}}_i]_k = \begin{pmatrix} \mathbf{h}_{i,1}[k] \\ \vdots \\ \mathbf{h}_{i,N_L}[k] \end{pmatrix} , \tag{5.18}$$

and

$$[\underline{\mathbf{h}}'_i]_k = \begin{pmatrix} \mathbf{h}'_{i,1}[k] \\ \vdots \\ \mathbf{h}'_{i,N_T}[k] \end{pmatrix} . \tag{5.19}$$

[9] I only describe spatial correlation at the transmitter side here. Since I assume the receive antennas to be spatially uncorrelated, the LMMSE estimator described in this section is still optimal in the LMMSE sense.

Assuming the channel to be spatially uncorrelated, i.e., $\mathbb{E}\{[\underline{\mathbf{h}}'_i]_k\,[\underline{\mathbf{h}}'_i]_k^H\} = \mathbf{I}_{N_T}$, the correlation matrix of the effective channel is given by

$$\mathbf{C}_{\mathbf{h}}^{(s)} = \mathbb{E}\{[\underline{\mathbf{h}}_i]_k\,[\underline{\mathbf{h}}_i]_k^H\} = \mathbf{F}^T\mathbf{F}^\star \;, \tag{5.20}$$

which essentially means that the precoder introduces spatial correlation on the effective channel. Due to the semi-unitary LTE-A codebook from [10], $\mathbf{F}^H\mathbf{F}$ is a diagonal matrix in any case and further, $\mathbf{F}^H\mathbf{F} = 1/N_L\mathbf{I}_{N_L}$ if $N_T = N_L$ which means that no correlation is introduced if the number of layers equals the number of transmit antennas.

5.3 Least-Squares Based Estimation

For an other method of estimation, a LS criterion is applied on (5.4) to obtain a channel estimate by solving

$$\tilde{\underline{\mathbf{h}}}_i = \arg\min_{\underline{\mathbf{h}}_i} \left\|\mathbf{y}_i - \underline{\underline{\mathbf{R}}}\underline{\mathbf{h}}_i\right\|_2^2 \;. \tag{5.21}$$

As $\underline{\underline{\mathbf{R}}} \in \mathbb{C}^{N_{\mathrm{SC}}\times N_L N_{\mathrm{SC}}}$ is a fat matrix, there is no unique solution to the underdetermined problem (5.21). Choosing the least-norm solution of $\underline{\mathbf{h}}_i$, the right pseudo-inverse of $\underline{\underline{\mathbf{R}}}$ is exploited to obtain

$$\tilde{\underline{\mathbf{h}}}_i = \underline{\underline{\mathbf{R}}}^H\left(\underline{\underline{\mathbf{R}}}\underline{\underline{\mathbf{R}}}^H\right)^{-1}\mathbf{y}_i \;, \tag{5.22}$$

as shown in Appendix A.3. Inserting (5.5) in (5.22) and exploiting (4.6) leads to

$$\begin{pmatrix} \tilde{\mathbf{h}}_{i,1} \\ \vdots \\ \tilde{\mathbf{h}}_{i,N_L} \end{pmatrix} = \begin{pmatrix} \mathbf{R}_1^H \\ \vdots \\ \mathbf{R}_{N_L}^H \end{pmatrix} \underbrace{\left(\sum_{l=1}^{N_L}\mathbf{R}_l\mathbf{R}_l^H\right)^{-1}}_{1/N_L\mathbf{I}} \mathbf{y}_i \;. \tag{5.23}$$

Considering the l^{th} row yields the LS channel estimate for the effective channel from transmit layer l to receive antenna i

$$\tilde{\mathbf{h}}_{i,l} = \frac{1}{N_L}\mathbf{R}_l^H\mathbf{y}_i \;, \tag{5.24}$$

showing, that LS estimation of all effective MIMO from any spatial layer l to a single receive antenna i is a decoupled problem.

Directly applying a layer-wise LS estimation for the channel $\mathbf{h}_{i,l}$ from layer l to receive antenna i is expressed by the minimization problem

$$\tilde{\mathbf{h}}_{i,l} = \arg\min_{\mathbf{h}_{i,l}} \left\|\mathbf{y}_i - \mathbf{R}_l\mathbf{h}_{i,l}\right\|_2^2 \;. \tag{5.25}$$

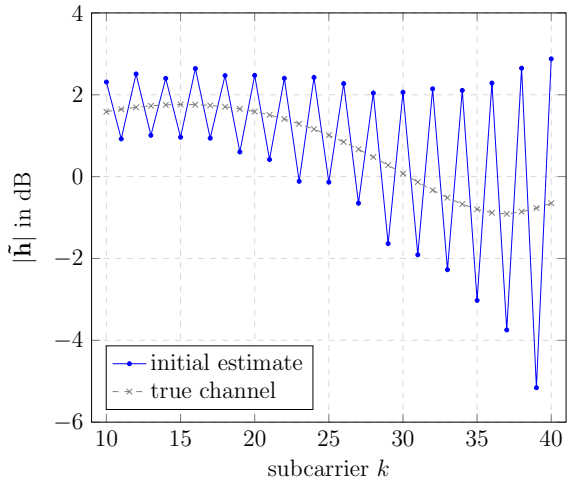

Figure 5: An exemplary snapshot of the initial channel estimate.

Since $\mathbf{R}_l \in \mathbb{C}^{N_{\mathrm{SC}} \times N_{\mathrm{SC}}}$, this problem is solved by the left pseudoinverse as shown in Appendix A.4.[10] Again exploiting (4.6) leads to

$$\tilde{\mathbf{h}}_{i,l} = \left(\mathbf{R}_l^H \mathbf{R}_l\right)^{-1} \mathbf{R}_l^H \mathbf{y}_i = \mathbf{R}_l^H \mathbf{y}_i \ . \tag{5.26}$$

which shows to be identical to (5.24), obtained by solving a LS problem for all effective MIMO channels at once, up to a factor $\frac{1}{N_L}$. Further this solution can be interpreted as follows. The effective MIMO channel from layer l to receive antenna i is obtained by multiplying the received signal on antenna i with the corresponding reference signal from layer l. (5.26) is therefore the initial step in LS based estimation and will be referred to as initial channel estimate in the sequel.

To further investigate on the initial estimate, the system model (5.3) is inserted in (5.26), yielding

$$\begin{aligned} \tilde{\mathbf{h}}_{i,l} =& \mathbf{R}_l^H \sum_{p=1}^{N_L} \mathbf{R}_p \mathbf{h}_{i,p} + \mathbf{R}_l^H \mathbf{z}_i \\ =& \mathbf{h}_{i,l} + \underbrace{\sum_{\substack{p=1 \\ p \neq l}}^{N_L} \mathbf{R}_l^H \mathbf{R}_p \mathbf{h}_{i,p}}_{\text{inter-layer interference}} + \check{\mathbf{z}}_i \ . \end{aligned} \tag{5.27}$$

[10] In this special case matrix $\mathbf{R}_l$ is actually invertable and the conventional inverse also solves the estimation problem.

Here $\check{\mathbf{z}}_i$ has the same distribution as $\mathbf{z}_i$ since $\mathbf{R}_l^H$ is unitary and introduces phase changes only. Due to the allocation of DMRS on the same time and frequency resources on different spatial layers, the initial estimate of one MIMO channel suffers from interference of other layers. This is expressed in the second term of (5.27) and will be referred to as inter-layer interference. An example of this initial estimate is shown in Fig. 5, illustrating that the interference in (5.26) is quite strong. The initial estimate is not directly applicable for coherent detection but requires further processing.

In this context it is obvious why inter-layer interference is not an issue on a frequency flat channel, i.e., $\mathbf{H}_{i,l} = h_{i,l}\mathbf{I}$. For this special case code-domain orthogonality is directly exploited as in (4.7), where evaluating the trace is exchanged by multiplication with the DMRS in vector form. In this manner, a channel estimate of a frequency flat channel is obtained by

$$\hat{h}_{i,l} = \frac{\mathbf{r}_l^H \mathbf{y}_i}{\mathbf{r}_l^H \mathbf{r}_l} \ . \tag{5.28}$$

This estimated channel coefficient is then valid for all subcarriers k. Inserting (5.27) and exploiting (4.7) yields

$$\begin{aligned} \hat{h}_{i,l} =& \frac{1}{N_{\mathrm{SC}}} \sum_{p=1}^{N_L} \mathbf{r}_l^H \mathbf{H}_{i,p} \mathbf{r}_p + \frac{1}{N_{\mathrm{SC}}} \mathbf{r}_l^H \mathbf{z}_i \\ =& h_{i,l} + \frac{1}{N_{\mathrm{SC}}} \mathbf{r}_l^H \mathbf{z}_i \ . \end{aligned} \tag{5.29}$$

This way, an estimate of a non frequency selective channel is obtained by directly applying DMRS orthogonality (4.7). With this method a single coefficient is estimated, meaning it leads to high estimation error when applied for estimating a channel with significant delay spread. In this case, methods exploiting DMRS code-domain orthogonality in a more sophisticated (piecewise) manner have to be utilized.

5.3.1 Discrete Fourier Transform based Estimation

A well known approach for CE in LTE-A uplink is DFT based estimation [23], which aims to separate the MIMO channels contributing to (5.27) in time domain. For this the individual cyclic shift of each DMRS is exploited. Applying a DFT on the receive signal, the individual phase shifts will translate into a shifts in time domain. This makes a separation of CIRs from different MIMO channels possible by windowing. Applying an IDFT on the initial

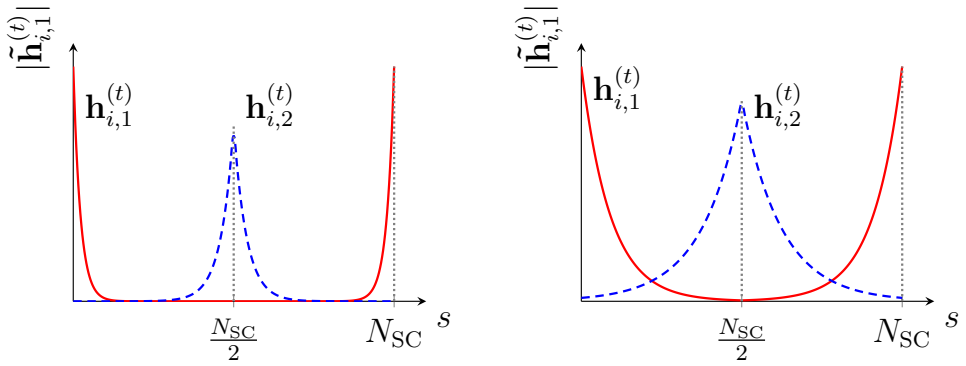

(a) Large bandwidth. (b) Small bandwidth.

Figure 6: CIR separation in time domain for $N_L = 2$.

estimate yields

$$\begin{aligned}\tilde{\mathbf{h}}_{i,l}^{(t)} =& \mathbf{D}_{N_{\mathrm{SC}}}^{H} \tilde{\mathbf{h}}_{i,l} \\ =& \mathbf{D}_{N_{\mathrm{SC}}}^{H} \sum_{p=1}^{N_L} \mathbf{T}_l^H \mathbf{T}_p \mathbf{D}_{N_{\mathrm{SC}}} \mathbf{h}_{i,p}^{(t)} + \mathbf{D}_{N_{\mathrm{SC}}}^{H} \tilde{\mathbf{z}}_i \\ =& \sum_{p=1}^{N_L} \mathbf{\Pi}^{\Delta N} \mathbf{h}_{i,p}^{(t)} + \mathbf{D}_{N_{\mathrm{SC}}}^{H} \tilde{\mathbf{z}}_i \ , \end{aligned} \tag{5.30}$$

with the permutation matrix $\mathbf{\Pi}$ which is obtained by cyclically left shifting the identity matrix as in [26]. The power of the permutation matrix is $\Delta N = \Delta\alpha_{l,p} N_{\mathrm{SC}}/2\pi$ and depends on the difference in phase shift between layers p and l from Section 4. The time domain estimate $\tilde{\mathbf{h}}_{i,l}^{(t)}$ consists of N_L CIRs, from all N_L active layers to receive antenna i. An example of $\tilde{\mathbf{h}}_{i,l}^{(t)}$ for two active spatial layers, and therefore $|\Delta\alpha_{1,2}| = \pi$, is shown in Fig. 6a. The two contributing CIRs, $\mathbf{h}_{i,1}^{(t)}$ from layer one and $\mathbf{h}_{i,2}^{(t)}$ from layer two, are illustrated in red and blue respectively. Due to the cyclic shift of DMRS, these N_L contributions are shifted relative to each other such that the distance in time between them is maximized. The intended CIR, from layer one, is centred around the origin and can be separated by windowing. In case of a narrow transmission bandwidth or a long CIR, the time domain MIMO channels overlap, cf. Fig. 6b, which is referred to as CIR leakage. DFT based CE therefore leads to inferior performance for small scheduled user bandwidths or channels with high delay spread.

To separate the different MIMO channels, windowing with window size

2β is carried out

$$\check{\mathbf{h}}_{i,l}^{(t)}[s] = \begin{cases} \tilde{\mathbf{h}}_{i,l}^{(t)}[s] & \text{for } s < \beta \text{ or } s > N_{\mathrm{SC}} - \beta \\ 0 & \text{otherwise ,} \end{cases} \tag{5.31}$$

where β is chosen to be the CP length N_{CP}. To yield a frequency domain CE, a DFT is applied on the separated CIR

$$\hat{\mathbf{h}}_{i,l}^{\mathrm{DFT}} = \mathbf{D}_{N_{\mathrm{SC}}} \check{\mathbf{h}}_{i,l}^{(t)} \ . \tag{5.32}$$

5.3.2 Averaging

When CIRs are separated in time domain, and the CIR length is big compared to the scheduled user bandwidth, CIR leakage occurs as described above. The idea I introduced in [3] is to cancel inter-layer interference in the initial estimate (5.26) by post processing in frequency domain. In this section the method of interference cancellation by averaging is explained.

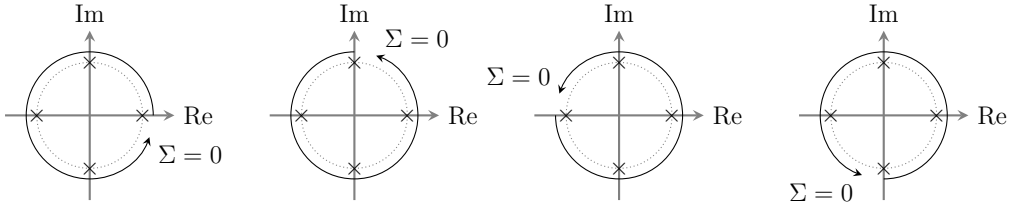

Figure 7: The inter-layer interference on the unit circle is cancelled when summed over all points.

Concluding from (4.6), the interference in (5.27) is characterized by a rotation on the unit circle in the complex plane as illustrated in Fig. 7. The phase shift between two adjacent points in frequency is determined by $\Delta\alpha_{p,l}$ and the number of distinct points on the unit circle is given by $\gamma = 2\pi/\Delta\alpha_{p,l}$. The phase shift $\Delta\alpha_{p,l} = \alpha_p - \alpha_l$ and therefore the periodicity γ of the interference is dependent on the two layers p and l. Exploiting (4.4) and (4.5) in combination with Table 1, a relation between $\Delta\alpha_{p,l}$ and the two layers l and p is found, as illustrated in Fig. 8. This figure is interpreted as follows: By selecting two vertices of different layers l, the label of the corresponding edge connecting these two vertices gives the phase shift $\Delta\alpha_{p,l}$ between these layers. This relation turns out to be independent of the actual cyclic shift field from uplink related DCI.

When estimating all MIMO channels exploiting (5.27) all possible combinations of $p, l \in \{1, \ldots, N_L\}$ appear and therefore different values of $\Delta\alpha_{p,l}$ will

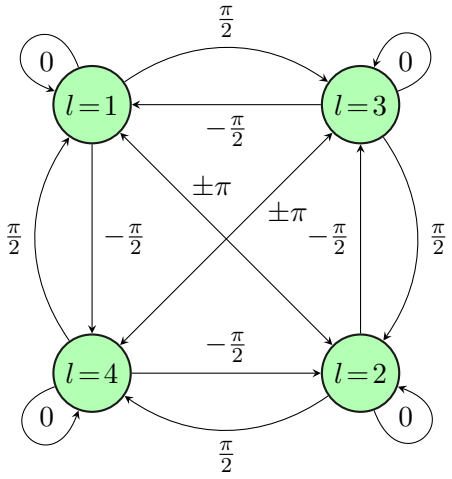

Figure 8: Layer dependent phase shift.

occur in the inter-layer interference term. In order to cancel all interference terms at once the sum over the largest possible number of points on the unit circle, i.e., the largest possibly occurring periodicity, has to be calculated. This periodicity is determined by the minimum phase shift between two different layers which is given by

$$\Delta\alpha_{\min} = \begin{cases} \min_{\substack{l,p\in\{1,\ldots,N_L\} \\ l\neq q}} |\Delta\alpha_{p,l}| & \text{for } 2 \leq N_L \leq 4 \\ 2\pi & \text{for } N_L = 1 \end{cases} . \tag{5.33}$$

As explained in Section 5.3.1, this phase shift determines MIMO channel component separability. When $\Delta\alpha_{\min}$ is small, e.g. when four transmission layers are active, frequency selective channels are unlikely to be separable and inter-layer interference is inevitable.

The corresponding (maximum) periodicity is then

$$\bar{\gamma} = \frac{2\pi}{\Delta\alpha_{\min}} . \tag{5.34}$$

From Fig. 8 it is obvious that $\bar{\gamma} = 4$ as soon as more than two spatial layers are active, i.e., for $N_L \geq 3$. The corresponding values of $\bar{\gamma}$ are listed in Table 2.

Concluding from this, the sum of $\bar{\gamma}$ consecutive elements in (4.6) will evaluate to zero, independent of the actual layers p and l. In terms of interference cancellation the key observation is, that the sum of $\bar{\gamma}$ consecutive elements in (4.6) will evaluate to zero. Therefore, averaging (5.26) over a complete turn on the unit circle will cancel the interference, as indicated in Fig. 7. For

Table 2: Phase shift for possible numbers of layers N_L.

N_L	$\Delta\alpha_{\min}$	$\bar{\gamma}$	$\Delta\alpha_{p,l}$
1	2π	1	$\{2\pi\}$
2	π	2	$\{\pm\pi, 2\pi\}$
3	$\frac{\pi}{2}$	4	$\{\pm\frac{\pi}{2}, \pm\pi, 2\pi\}$
4	$\frac{\pi}{2}$	4	$\{\pm\frac{\pi}{2}, \pm\pi, 2\pi\}$

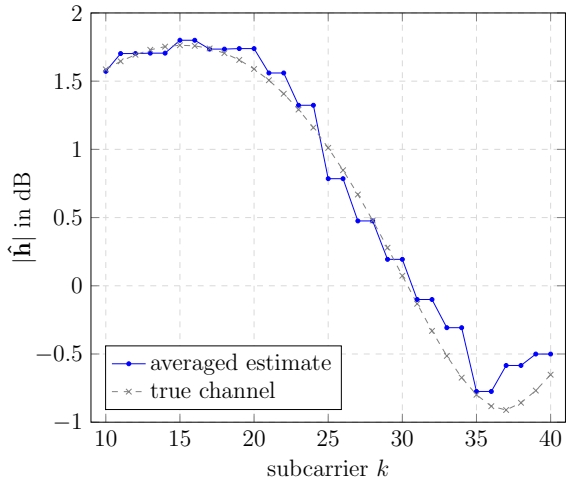

Figure 9: An exemplary snapshot of the averaged channel estimate for $\bar{\gamma} = 2$.

the averaging CE method the sum, or average, over γ consecutive elements of $\tilde{\mathbf{h}}_{i,l}$ is calculated. This is identical to saying the FD-CDM orthogonality is preserved when the channel is assumed to be constant on $\bar{\gamma}$ consecutive subcarriers [34]. The channel estimate is obtained by piecewise averaging the initially obtained estimate over $\bar{\gamma}$ adjacent elements as

$$\hat{\mathbf{h}}_{i,l}^{\mathrm{AV}}[k] = \frac{1}{\bar{\gamma}} \sum_{j=\lceil \frac{k}{\bar{\gamma}} \rceil \bar{\gamma} - \bar{\gamma} + 1}^{\lceil \frac{k}{\bar{\gamma}} \rceil \bar{\gamma}} \tilde{\mathbf{h}}_{i,l}[j] \ . \tag{5.35}$$

This results in a piecewise averaged channel estimate that is constant on $\bar{\gamma}$ consecutive subcarriers as shown in Fig. 9.

On a frequency flat channel, piecewise averaging is not an issue since there is no frequency selective shape that has to be preserved. In this special case averaging over the whole scheduled bandwidth is carried out to obtain the channel coefficient of the frequency flat channel. Applying this average

on (5.27) yields

$$\begin{aligned}\hat{h}_{i,l} =& \frac{1}{N_{\mathrm{SC}}} \operatorname{trace}\left(\mathbf{R}_l^H \sum_{p=1}^{N_L} \mathbf{R}_p \mathbf{h}_{i,p} + \mathbf{R}_l^H \mathbf{z}_i\right) \\ =& \frac{1}{N_{\mathrm{SC}}} \sum_{u=1}^{N_L} \mathbf{r}_l^H \mathbf{H}_{i,p} \mathbf{r}_p + \frac{1}{N_{\mathrm{SC}}} \mathbf{r}_l^H \mathbf{z}_i \\ =& h_{i,l} + \frac{1}{N_{\mathrm{SC}}} \mathbf{r}_l^H \mathbf{z}_i \end{aligned} \tag{5.36}$$

where (4.7) was exploited and the frequency flat channel is inserted as $\mathbf{H}_{i,l} = h_{i,l}\mathbf{I}_{N_{\mathrm{SC}}}$. However, that is exactly the solution obtained by (5.28). This means, in the case of a frequency selective channel, this orthogonality is exploited in a piecewise manner, assuming the channel coefficients on $\bar{\gamma}$ adjacent subcarriers to be equal, while orthogonality can be exploited directly on a frequency flat channel.

For interference cancellation it suffices to sum over all points of interference on the unit circle while it actually does not matter where the summation starts and stops as illustrated in Fig. 7. The method of averaging is therefore augmented to a sliding average. Here, the averaging window of size $\bar{\gamma}$ is shifted subcarrier by subcarrier over the scheduled bandwidth. The sliding average is given by[11]

$$\hat{\mathbf{h}}_{i,l}^{\mathrm{SAV}}[k] = \frac{1}{\bar{\gamma}^2} \sum_{t=k-\bar{\gamma}+1}^{k} \sum_{j=t}^{t+\bar{\gamma}-1} \tilde{\mathbf{h}}_{i,l}[j] \quad \text{for } \bar{\gamma} \leq k \leq N_{\mathrm{SC}} - \bar{\gamma} + 1 \ . \tag{5.37}$$

Here, the second sum describes the averaging of $\bar{\gamma}$ elements while the first sum describes the shift of the averaging window. Exploiting the sliding average, the channel estimate is not piecewise constant any more and changes from subcarrier to subcarrier as shown in Fig. 10. Further, as more elements of $\tilde{\mathbf{h}}_{i,l}$ are averaged to obtain one coefficient of $\hat{\mathbf{h}}_{i,l}^{\mathrm{SAV}}$, compared to (5.35), noise influence is suppressed more effectively.

As complexity of both, averaging and sliding averaging, is asymptotically linear, i.e., $\mathcal{O}(N_{\mathrm{SC}})$, and the performance of sliding averaging is superior for reasons explained above, the method of averaging is considered as intermediate step to sliding averaging.

[11] Please note that in this definition the range of subcarriers k is limited to a region of subcarriers k, where the averaging window is not limited by band borders in order to increase readability. An equation for sliding averaging including band borders, i.e., for $k \in \{1, \ldots, N_{\mathrm{SC}}\}$, is given in Appendix A.5.

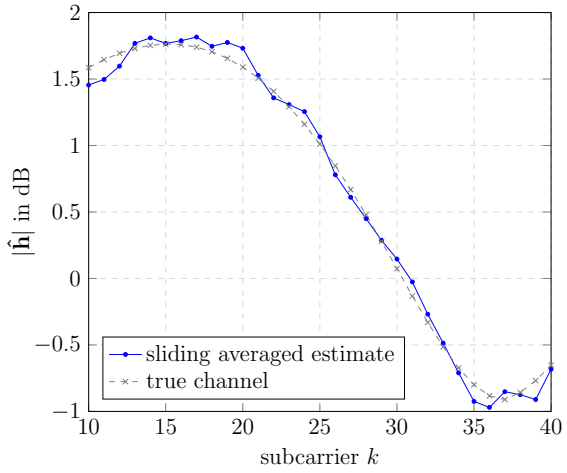

Figure 10: An exemplary snapshot of the sliding averaged channel estimate.

5.3.3 Quadratic Smoothing

The estimation method described in the previous section shows that applying a sliding averaging to the initial channel estimate, obtained as the solution to an LS estimation problem, yields a well performing channel estimation method [1, 3, 35]. Similar effects are achieved when the initial LS problem is augmented by a smoothing regularization. By applying Quadratic Smoothing (QS) [36], the difference in channel coefficients of neighbouring subcarriers is penalized within the minimization problem. This regularization is justified since adjacent subcarriers will be correlated in a frequency selective channel.

The quadratic smoothing is expressed with the matrix $\mathbf{Q} \in \mathbb{R}^{(N_{\mathrm{SC}}-1)\times N_{\mathrm{SC}}}$

$$\mathbf{Q} = \begin{pmatrix} -1 & 1 & & & \\ & -1 & 1 & & \\ & & \ddots & \ddots & \\ & & & -1 & 1 \end{pmatrix}, \tag{5.38}$$

capturing the regularization on the difference between neighbouring channel coefficients. The regularized LS problem is then given by

$$\hat{\mathbf{h}}_{i,l}^{\mathrm{QS}} = \arg\min_{\mathbf{h}_{i,l}} \left\| \mathbf{y}_i - \mathbf{R}_l \mathbf{h}_{i,l} \right\|_2^2 + \lambda \left\| \mathbf{Q}\mathbf{h}_{i,l} \right\|_2^2 , \tag{5.39}$$

with the trade-off, or frequency smoothing parameter λ. The solution to this optimization problem from [36] is

$$\hat{\mathbf{h}}_{i,l}^{\mathrm{QS}} = \left(\mathbf{I}_{N_{\mathrm{SC}}} + \lambda \mathbf{Q}^H \mathbf{Q} \right)^{-1} \underbrace{\mathbf{R}_l^H \mathbf{y}_i}_{\tilde{\mathbf{h}}_{i,l}} , \tag{5.40}$$

as shown in Appendix A.6. The smoothing parameter λ reflects the frequency selectivity of the channel. A high value of λ lies emphasis on the smoothing, leading to a good performance at low Signal to Noise Ratio (SNR). If however, smoothing is chosen too dominant, a very frequency selective channel will be smoothed out, leading again to a high estimation MSE. The optimal value of smoothing parameter λ is therefore crucial for the performance of the QS estimator. As finding a suited value λ is dependent on the actual frequency selectivity of the channel, the smoothing parameter can be interpreted as a prior about the channel [37].

Further, as explained in Section 4, the inter-layer interference, and especially its periodicity, is dependent on the number of active spatial layers. As already explained in Section 5.3.2, when two layers are employed, averaging is carried out over two consecutive subbarriers, and for three or four active spatial layers, the channel estimate is averaged over four adjacent subcarriers. For QS estimation this means, that the smoothing parameter not only depends on the channel's frequency selectivity but also on the number of employed spatial layers N_L. The smoothing parameter λ therefore influences the trade-off between smoothing the channel estimate while preserving its frequency selective nature, as well it influences the reduction of inter-layer interference.

One way of choosing the smoothing parameter proposed by [36] is finding the optimal trade-off between $\left\|\mathbf{y}_i - \mathbf{R}_l \mathbf{h}_{i,l}\right\|_2$ and $\left\|\mathbf{Q}\mathbf{h}_{i,l}\right\|_2$. This yields a λ, leading to a balance between the original LS term and the regularization term in (5.39). This is however not equal to minimizing the estimation MSE with respect to λ. To obtain a smoothing parameter that ideally leads to a minimum MSE for channels with a wide range of delay spread, I compare CE MSE dependent on λ on a Pedestrian A (PedA), Typical Urban (TU) and Vehicular B (VehB) channel [38, 39], as listed in Table 3. Here the fundamental relation between channel coherence bandwidth B_{coh} and Root Mean Square (RMS) delay spread τ_{RMS} is known [40] to be

$$B_{\text{coh}} \approx \frac{1}{2\pi\tau_{\text{RMS}}} \,. \tag{5.41}$$

Simulation results in terms of MSE dependent on λ for all three proposed channel models are shown in Fig. 11. Since the smoothing parameter depends on the number of employed layers, two spatial layers are employed in Fig. 11a while four spatial layers are active in Fig. 11b. A clear optimum for λ is observed for the TU channel. Too little smoothing leads to insufficient noise cancelling, too much smoothing destroys the frequency selective channel. In case of the PedA there is no such optimum. Since the channel is almost frequency flat, there is no over-smoothing. In case of VehB, the assumption

Table 3: RMS delay spread and coherence bandwidth of employed channel models.

Channel Model	τ_{RMS}	B_{coh}
PedA	45 ns	3536.8 kHz
TU	500 ns	318.3 kHz
VehB	4000 ns	39.8 kHz

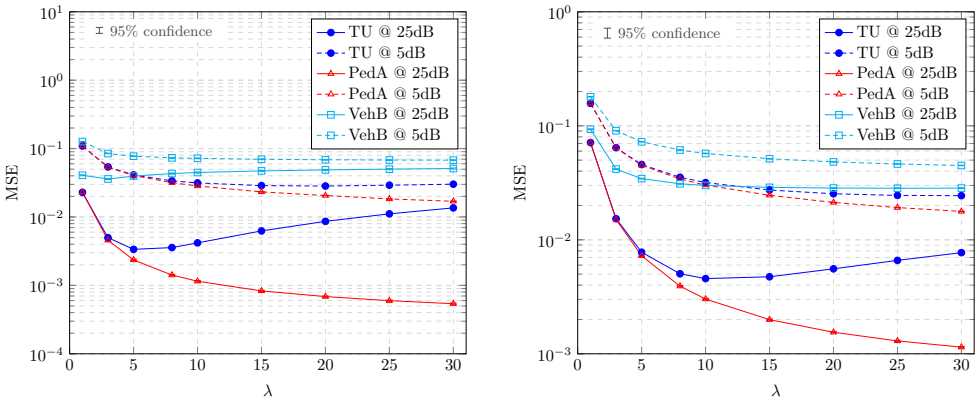

(a) With two active spatial layers. (b) With four active spatial layers.

Figure 11: Smoothing parameter choice.

of uncorrelated subcarriers is not fulfilled as it has a very small coherence bandwidth, c.f. Table 3.[12] For higher λ somehow the channel estimate is smoothed out and the mean is fitted to the actual channel, therefore the MSE is decreasing slowly with λ.

Based on this results, I chose $\lambda = 8$ for $N_L = 2$ and $\lambda = 15$ for $N_L = \{3, 4\}$. Of course when only a single spatial layer is active, λ is set to zero to obtain a plain LS estimator. Since there is no inter-layer interference in this case, there is also no need for averaging or smoothing. In this way the smoothing parameter is fixed irrespective of the actual channel characteristics in order to obtain an estimation method that does not require prior channel knowledge, although an adaptive value of λ would improve the overall estimation performance. Also in [28], where quadratic averaging is employed in a different context, authors claim that λ is approximately constant.

Similar to (5.37), QS can be interpreted as another way to cope with the

[12] Please note that simulation results for VehB were obtained with extended CP length as the CIR exceeds the normal CP length. Although a VehB's CIR is even slightly longer than the extended CP length, the resulting interference is negligible.

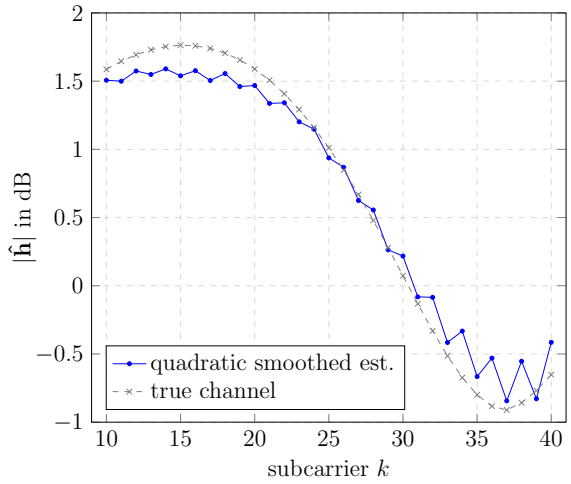

Figure 12: An exemplary snapshot of the quadratically smoothed channel estimate.

inter-layer interference in (5.27) by post processing. This method does not use the DMRS structure explicitly but suppresses the interference by smoothing. It is therefore not able to cancel the complete inter-layer interference as depicted in Fig. 12.

5.3.4 Approximate Quadratic Smoothing

Although the smoothing parameter within the QS estimator is fixed such that this algorithm does not require any prior about the channel, (5.40) requires a matrix inverse leading to high asymptotic complexity of $\mathcal{O}(N_{\mathrm{SC}}^3)$. To reduce the computational complexity I exploit the strong structure within this matrix inverse and thereby propose an approximate quadratic smoothing estimator in this section.

The matrix to be inverted for QS estimation (5.40) is a symmetric tri-diagonal matrix and given by

$$\mathbf{B} = \mathbf{I}_{N_{\mathrm{SC}}} + \lambda \mathbf{Q}^H \mathbf{Q} = \begin{pmatrix} 1+\lambda & -\lambda & & & & \\ -\lambda & 1+2\lambda & -\lambda & & & \\ & \ddots & \ddots & \ddots & & \\ & & -\lambda & 1+2\lambda & -\lambda & \\ & & & -\lambda & 1+\lambda \end{pmatrix} . \quad (5.42)$$

By approximating the first and last element of the main diagonal, i.e., $\mathbf{B}[1,1]$ and $\mathbf{B}[N_{\mathrm{SC}}, N_{\mathrm{SC}}]$ respectively, a symmetric tri-diagonal Toeplitz matrix $\tilde{\mathbf{B}}$ is

obtained as

$$\tilde{\mathbf{B}} = \begin{pmatrix} 1+2\lambda & -\lambda & & & & \\ -\lambda & 1+2\lambda & -\lambda & & & \\ & \ddots & \ddots & \ddots & & \\ & & -\lambda & 1+2\lambda & -\lambda & \\ & & & -\lambda & 1+2\lambda & \end{pmatrix} . \tag{5.43}$$

For such a matrix, expressions for the matrix inverse are known [41]. Whether this approximation leads to an approximate inverse $\tilde{\mathbf{B}}^{-1}$ that is significantly different from $\mathbf{B}^{-1}$ depends on the size of $\mathbf{B}$, given by N_{SC}, and the smoothing factor λ. However, assuming a user is scheduled at least one RB, N_{SC} is at least 12 subcarriers. In this worst case, only two out of 34 non-zero elements in $\mathbf{B}$ are modified to obtain $\tilde{\mathbf{B}}$.

Since $\tilde{\mathbf{B}}$ is now a tri-diagonal Toeplitz matrix, the inverse can be calculated analytically as described in Appendix A.7. Exploiting (A.25) to calculate the inverse of $\tilde{\mathbf{B}}$ leads to

$$\tilde{\mathbf{B}}^{-1}[i,j] = \begin{cases} \frac{1}{\lambda}\frac{U_{i-1}(d)U_{N-j}(d)}{U_N(d)} & \text{for } i \leq j \ , \\ \frac{1}{\lambda}\frac{U_{j-1}(d)U_{N-i}(d)}{U_N(d)} & \text{for } i > j \ , \end{cases} \tag{5.44}$$

with $d = 1 + \frac{1}{2\lambda}$. The matrix inverse is a symmetric matrix and reads as

$$\tilde{\mathbf{B}}^{-1} = \frac{1}{\lambda U_N} \begin{pmatrix} U_0U_{N-1} & U_0U_{N-2} & U_0U_{N-3} & \dots & U_0U_2 & U_0U_1 & U_0U_0 \\ U_0U_{N-2} & U_1U_{N-2} & U_1U_{N-3} & \dots & U_1U_2 & U_1U_1 & U_1U_0 \\ U_0U_{N-3} & U_1U_{N-3} & U_2U_{N-3} & \dots & U_2U_2 & U_2U_1 & U_2U_0 \\ \vdots & \vdots & \vdots & \ddots & \vdots & \vdots & \vdots \\ U_0U_2 & U_1U_2 & U_2U_2 & \dots & U_{N-3}U_2 & U_{N-3}U_1 & U_{N-3}U_0 \\ U_0U_1 & U_1U_1 & U_2U_1 & \dots & U_{N-3}U_1 & U_{N-2}U_1 & U_{N-2}U_0 \\ U_0U_0 & U_1U_0 & U_2U_0 & \dots & U_{N-3}U_0 & U_{N-2}U_0 & U_{N-1}U_0 \end{pmatrix} , \tag{5.45}$$

where the argument of the Chebyshev polynomial $U(d)$ was omitted for readability.

Since all Chebyshev polynomials have to be evaluated for the same argument d, calculating the function values $U_0(d), \dots, U_{N_{\mathrm{SC}}}(d)$ is sufficient for determining the complete matrix. These values are determined in a recursive fashion, exploiting the recurrence relation

$$\begin{aligned} U_0(x) &= 1 \\ U_1(x) &= 2x \\ U_n(x) &= 2xU_n(x) - U_{n-1}(x) \ . \end{aligned} \tag{5.46}$$

Further one observes that diagonals of $\tilde{\mathbf{B}}^{-1}$ are approximately equal. This is intuitive because the smoothing of the initial channel estimate should

not depend on the actual subcarrier, which means that the applied post processing matrix should be close to a symmetric and Toeplitz structured matrix. Considering this observation, matrix $\tilde{\mathbf{B}}^{-1}$ is approximated by a Toeplitz matrix that is determined by the first column (or first row) of $\tilde{\mathbf{B}}^{-1}$, c.f. (5.45), which yields

$$\check{\mathbf{A}} = \frac{U_0}{\lambda U_N} \begin{pmatrix} U_{N-1} & U_{N-2} & \dots & \dots & U_1 & U_0 \\ U_{N-2} & U_{N-1} & U_{N-2} & & & U_1 \\ \vdots & U_{N-2} & U_{N-1} & U_{N-2} & & \vdots \\ \vdots & & \ddots & \ddots & \ddots & \vdots \\ U_1 & & & U_{N-2} & U_{N-1} & U_{N-2} \\ U_0 & U_1 & \dots & \dots & U_{N-2} & U_{N-1} \end{pmatrix} , \tag{5.47}$$

where the scaling factor U_0 was pulled in front of the matrix. To obtain a matrix that represents an averaging function, the rows of $\check{\mathbf{A}}$ have to be normalized. This yields the approximate quadratic smoothing estimator

$$\mathbf{A}^{\mathrm{AQS}}[i,j] = \frac{\check{\mathbf{A}}[i,j]}{\sum_{n=1}^{N} \check{\mathbf{A}}[i,n]} \qquad \forall n \in \{1,\dots,N_{\mathrm{SC}}\} \ . \tag{5.48}$$

A channel estimate is then obtained by

$$\hat{\mathbf{h}}_{i,l}^{\mathrm{AQS}} = \mathbf{A}^{\mathrm{AQS}} \tilde{\mathbf{h}}_{i,l} \ . \tag{5.49}$$

To evaluate the quality of this approximation, simulations are carried out. Figure 13 shows MSE over SNR for two and four active spatial layer obtained with QS and approximate QS. Results show that the obtained estimation error is almost the same for these two methods. For $N_L = 4$, approximate QS even attains a slightly lower MSE floor at high SNR.

By avoiding the computation of a matrix inverse, the complexity of approximate QS estimation is reduced to $\mathcal{O}(N_{\mathrm{SC}}^2)$, compared to cubic complexity to the initial QS scheme. The complexity is reduced even further, when lower order Chebyshev polynomials are neglected compared to the higher order polynomials in (5.47), yielding a band-diagonal matrix. The computation of such a matrix, as well as multiplying the initial channel estimate with this matrix leads to an asymptotic linear complexity, i.e., $\mathcal{O}(N_{\mathrm{SC}})$.

5.4 Simulation Results

In this section, the introduced CE methods are further analysed and compared by means of simulation results in terms of MSE and BER. Computer simulations were carried out with the MATLAB based Vienna LTE-A Uplink

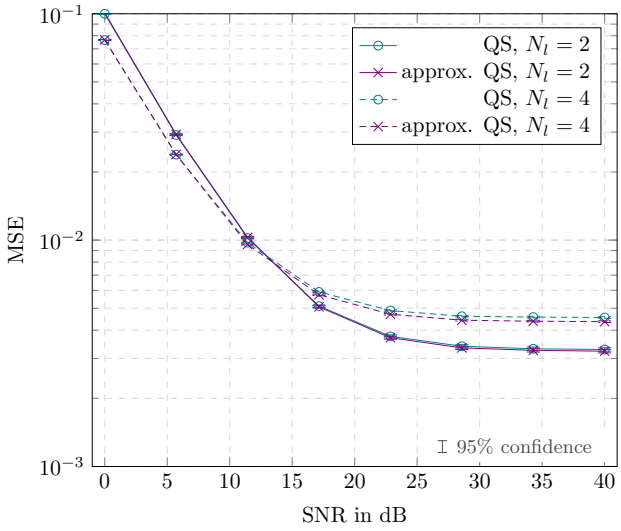

Figure 13: Comparison of quadratic smoothing and approximate quadratic smoothing for $N_L = 2$ and $N_L = 4$ on a TU channel.

Link Level Simulator [1, 42, 43] with simulation parameters as listed in Table 4. Since up to know only estimation of frequency selective channels is discussed, a block-fading assumption was made for simulations in this section, meaning the channel does not vary in time for the duration of a subframe. The channel is estimated, exploiting the introduced estimation algorithms, at pilot positions. Coefficients of the estimated channel in between reference symbol positions are obtained by extrapolating/repeating the estimated channel, which is obtained at symbol time $n = \{4, 11\}$, for the rest of the corresponding slot, which is expressed as

$$\hat{\mathbf{h}}_n[k] = \begin{cases} \hat{\mathbf{h}}_4[k] & \text{for } n \in \{1, \ldots, 7\}, \\ \hat{\mathbf{h}}_{11}[k] & \text{for } n \in \{8, \ldots, 14\}, \end{cases} \quad \forall k \in \{1, \ldots, N_{\mathrm{SC}}\} \ . \tag{5.50}$$

The CE MSE is then calculated as explained in Appendix A.8.

A performance comparison of estimation algorithms described in this section is shown in Fig. 14, where Fig. 14a and Fig. 14b show estimation MSE for two and four active spatial layers, respectively while Fig. 14c and Fig. 14d show the corresponding BER.

LMMSE estimation, as described in Section 5.2, serves as a performance reference as is achieves the lowest MSE of all linear estimators and is denoted by *MMSE*. Due to this purpose, second order channel and noise statistics are assumed to be perfectly known. Further, considering its asymptotic cubic complexity, i.e., $\mathcal{O}(N_{\mathrm{SC}}^3)$, and the fact that second order statistics need to be estimated render the LMMSE estimator rather impractical.

Table 4: Simulation parameters.

Parameter	Value
Simulated Subframes	1000
Channel Model	TU
Time-Fading Model	Block-Fading
Bandwidth	1.4 MHz ($N_{\mathrm{SC}} = 72$)
Symbol Alphabet	16 QAM
Antenna Configurations	2×2, $N_L = 2$
	4×4, $N_L = 4$
Equalizer	MMSE

Estimation based on DFT, as introduced in Section 5.3.1, aims to separate all MIMO CIRs in time domain. The corresponding simulation results in Fig. 14 are labelled *DFT*. In terms of MSE, results show that frequency selective channels cannot be fully separated in time domain and severe CIR leakage manifests in a rather high MSE floor. Comparing Fig. 14a and Fig. 14b this effect is even more pronounced when more than two spatial layers are active, since the shift between individual CIRs is significantly smaller. In either case, the MSE floor results in a high BER floor for DFT based CE. This estimation algorithm is therefore not applicable for MIMO transmissions over frequency selective channels.

Sliding average CE is described in Section 5.3.2 and labelled *SAV*. As this methods aims to cancel inter-layer interference of the initial estimate, results show a LS like performance up to high SNR. Only when the MSE is not dominated by noise contributions at very high values of SNR, the residual interference causes an MSE floor. This effect is more dominant for four transmission layers as there are more inter-layer interference components. Again this leads also to a non vanishing BER in the high SNR region for $N_L = 4$, however, the BER saturates at a low value.

CE according to Section 5.3.3 is referred to as quadratic smoothing and is labelled *QS*. This estimator is the solution to a regularized LS problem where the parameter λ determines the regularization trade-off or the degree of smoothing. The smoothing property means that more than just two our four channel coefficients (compared to sliding averaging estimation) of the initial estimate are averaged to obtain a single post processed channel coefficient. This is obvious from the estimator (5.40), which is determined by a matrix inverse that leads to a matrix containing only non-zero elements. Performance in the low SNR region is therefore very good in terms of MSE and BER as the smoothing leads to noise cancellation. At a high SNR region however,

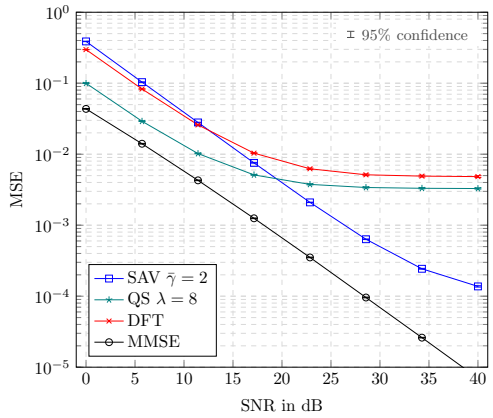

(a) MSE for $N_L = 2$.

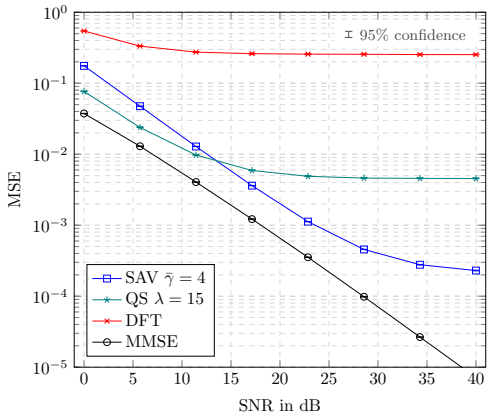

(b) MSE for $N_L = 4$.

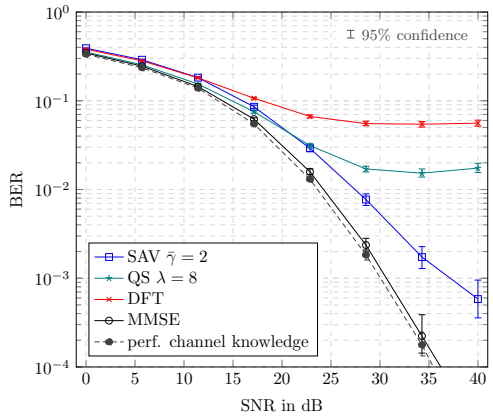

(c) Uncoded BER for $N_L = 2$.

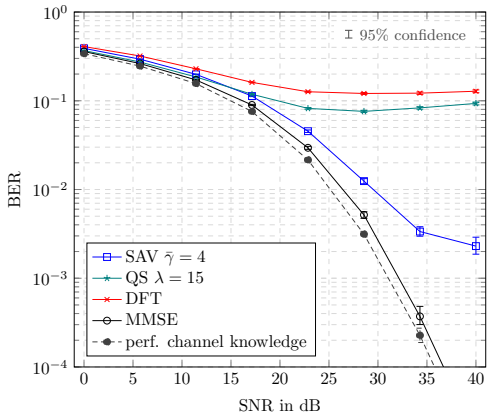

(d) Uncoded BER for $N_L = 4$.

Figure 14: Comparison of estimation methods for SU-MIMO on a TU channel and 16QAM.

quadratic smoothing results in a high residual MSE since this estimation method does actually not consider the reference symbol structure. It is therefore not able to cancel the inter-layer interference sufficiently which results in a MSE and BER floor.

For further investigation on the ability of MIMO channel separation, I compare sliding averaging estimation, quadratic smoothing estimation and DFT based CE for different transmission bandwidths. In Fig. 15 estimation MSE for two different bandwidths, obtained with before mentioned estimation methods is shown. A large bandwidth is chosen by assigning a user all 6 RBs, which corresponds to $N_{\mathrm{SC}} = 72$ and a small bandwidth here means a user is scheduled 2 consecutive RBs, corresponding to $N_{\mathrm{SC}} = 24$. Results show that sliding averaging estimation performs equally for a wide and a

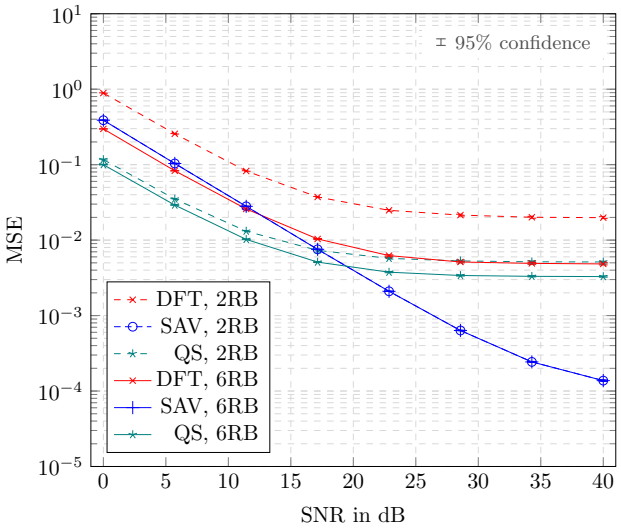

Figure 15: Comparison of estimation methods for different scheduled user bandwidths for a 2×2 transmission with $N_L = 2$.

narrow transmission bandwidth. The impact of bandwidth in quadratic smoothing estimation also shows to be very small. For DFT based estimation however, the MSE significantly increases when the bandwidth is reduced. This corresponds to the fact that CIR leakage increases with decreasing bandwidth and channel separation in time domain is deteriorated. DFT based CE results in a high error floor when a narrow transmission band is employed [20]. Both other introduced estimation algorithms show robust behavior on narrow transmission bands, as they do not separate MIMO channels in time domain.

6 Multi-User MIMO Channel Estimation

For SU-MIMO transmissions, as considered up to now, resources are assigned to a single user exclusively. This UE then transmits up to four spatial layers in the LTE-A uplink. For this mode of operation, a user is required to have more than one transmit antenna and as many transmitter chains, meaning complex and power hungry UE hardware. Further, antenna correlation has strong impact on MIMO gain [44] and integrating multiple antennas into a small hand-held device is challenging.

When the number of receive antennas at the Base Station (BS) exceeds the number of transmit antennas at the UE, improvements in sum throughput are reached when MU-MIMO operation is employed for uplink transmissions [45, 46]. In this case, multiple users are assigned the same resources and therefore transmit on the same time-frequency resources simultaneously. Exploiting multiple receive antennas, the BS then separates the received signals in the spatial domain.

In terms of detection, SU-MIMO and MU-MIMO are very similar, since the receiver has to separate and detect multiple spatial streams. Since these spatial layers stem from different UEs in the MU-MIMO case, the problem of CE is different from SU-MIMO operation in the LTE-A uplink. When received spatial streams, and also received DMRS correspondingly, originate from different users, orthogonality of reference signals has to be ensured not only between layers of the same user but also between different UEs. For this, the DMRS structure is further exploited and signalling of DCI from BS to the UE plays a key role.

CE for MU-MIMO transmissions in the LTE uplink was considered by many authors [16, 20, 24–26], where again DFT and DCT based estimation methods are very popular but suffer from CIR leakage. Corresponding changes of the DMRS are discussed in [11, 12] while the method of OCC is shown in [24].

In this section I first introduce a MU-MIMO system model, based on the model from Section 3. Then possibilities of separating received DMRS in time and frequency domain are discussed, focusing on the case of user with a single transmit antenna. Finally CE for UEs equipped with more than one transmit antenna is discussed.

6.1 System Model

For MU-MIMO I assume N_u users that are assigned the same N_{SC} subcarriers within a slot. Further, each UE is equipped with a single transmit antenna, enabling transmissions on a single spatial layer only. A system model is

therefore very similar to the model introduced in Section 3.

The modulated symbols at OFDM symbol time n, for all N_{SC} subcarriers of user u are described by vector $\mathbf{x}_{n,u} \in \mathcal{A}^{N_{\mathrm{SC}} \times 1}$. Stacking data vectors from all users $u \in \{1, \ldots, N_u\}$ yields

$$\mathbf{x}_n = \begin{pmatrix} \mathbf{x}_{n,1} \\ \mathbf{x}_{n,2} \\ \vdots \\ \mathbf{x}_{n,N_u} \end{pmatrix} \in \mathcal{A}^{N_{\mathrm{SC}} N_u \times 1} \ , \tag{6.1}$$

similar to (3.10). In the case of a single transmit antenna per UE, the system model (3.11) is adopted for MU-MIMO by substituting the layer index l with user index u as well as the number of layers N_L with the number of users N_u accordingly. A transmission model therefore reads as

$$\hat{\mathbf{x}}_n = \left(\mathbf{I}_{N_u} \otimes \mathbf{D}_{N_{\mathrm{SC}}}^H\right) \mathbf{G}_n \mathbf{H}_n \left(\mathbf{I}_{N_u} \otimes \mathbf{D}_{N_{\mathrm{SC}}}\right) \mathbf{x}_n + \left(\mathbf{I}_{N_u} \otimes \mathbf{D}_{N_{\mathrm{SC}}}^H\right) \mathbf{G}_n \mathbf{z}_n \ , \tag{6.2}$$

with the block-wise diagonal channel matrix

$$\mathbf{H}_n = \left(\mathbf{I}_{N_R} \otimes \mathbf{M}^H\right) \mathbf{H}_n^{(\mathrm{diag})} \left(\mathbf{I}_{N_u} \otimes \mathbf{M}\right) \in \mathbb{C}^{N_{\mathrm{SC}} N_R \times N_{\mathrm{SC}} N_u} \ . \tag{6.3}$$

The block-wise diagonal channel matrix $\mathbf{H}^{(\mathrm{diag})} \in \mathbb{C}^{N_{\mathrm{FFT}} N_R \times N_{\mathrm{FFT}} N_u}$, consisting of OFDM channel coefficients on the diagonals of the block matrices, includes all channels from N_u users to N_R receive antennas, similar to (3.7) . Channel matrix (6.3) is obtained similarly as the effective channel matrix from (3.7)-(3.9). For the Multi-User (MU) system model however, the channel is not called an effective channel as the precoding matrix of each user collapses to a scalar, i.e., $\mathbf{F} = 1$, since there is no precoding when a single spatial layer is transmitted per user.

As explained in Section 5, for the purpose of CE this model simplifies to an OFDM model. Similar to (5.1), a system description for CE is obtained by substituting the data vector $\mathbf{x}_n$ with the reference symbol vector $\tilde{\mathbf{r}}_n$ and removing the DFT spreading and de-spreading in (6.2). This leads to the stacked model for MU-MIMO CE, given by

$$\mathbf{y}_n = \mathbf{H}_n \tilde{\mathbf{r}}_n + \mathbf{z}_n \ . \tag{6.4}$$

Considering the i^{th} row of (6.4), the received signal on receive antenna i yields

$$\mathbf{y}_{m,i} = \left(\tilde{\mathbf{R}}_{m,1}^{S_1}, \ldots, \tilde{\mathbf{R}}_{m,1}^{S_{N_u}}\right) \begin{pmatrix} \mathbf{h}_{m,i,1} \\ \vdots \\ \mathbf{h}_{m,i,N_u} \end{pmatrix} + \mathbf{z}_{m,i} \ , \tag{6.5}$$

similar to (5.3). Here the time index n is substituted by the slot index $m \in \{1, 2\}$ since this model is only valid for OFDM symbol times where DMRS are multiplexed. Compared to (6.4), slot index $m = 1$ corresponds to symbol time $n = 4$ and slot $m = 2$ corresponds to time $n = 11$ respectively. Also the layer index l is set to $l = 1$ as each user only employs a single spatial layer. A definition of reference symbols $\tilde{\mathbf{R}}^{S_u}_{m,l}$ for MU-MIMO is given in the following.

6.2 Time Domain Orthogonality

For CE in MU-MIMO transmissions, DMRS are augmented by OCC compared to (4.2). This leads to additional orthogonality in time domain, as shown in [24]. While the already explained frequency domain orthogonality is reached by cyclic shifts, the concept of OCC leads to time domain orthogonality, allowing more flexibility in scheduling for MU-MIMO transmissions. While separating received reference signals in frequency domain by exploiting different cyclic shifts requires users to be scheduled on the same subcarriers, orthogonality in time domain is independent on scheduling in frequency domain [24]. The drawback of this method is, that similar to the frequency domain orthogonality, a time selective channel destroys orthogonality in general.

DMRS from (4.2) are augmented by the OCC $\mathbf{w}^S_l \in \{-1, 1\}^{2\times 1}$

$$\tilde{\mathbf{R}}^S_{m,l} = \mathbf{w}^S_l[m]\mathbf{T}^S_l \operatorname{Diag}(\bar{\mathbf{r}}) \ , \tag{6.6}$$

with the slot index $m \in \{1, 2\}$. Further, dependence on the CSF from uplink related DCI format is indicated by CSF S. Comparing with Table 1, a DMRS $\tilde{\mathbf{R}}^S_{m,l}$ now depends on the CSF S, the slot index m and the layer index l.

Assuming a block fading channel, meaning the channel is constant for the duration of a subframe, OCC can be exploited to separate two users in MU-MIMO transmissions. On such a channel, the vector $\mathbf{h}_{m,i,u}$ from (6.5) does not depend on the slot index m, which is therefore omitted in the following. Further, I assume two users, i.e., $N_u = 2$, both with a single transmit antenna. User $u = 1$ is assigned CSF S_1 and transmits on channel $\mathbf{h}_{i,1}$ and user $u = 2$ is assigned CSF S_2 and transmits on channel $\mathbf{h}_{i,2}$ to receive antenna i. As an example, the orthogonal sequences are chosen as

$$\mathbf{w}^{S_1}_1 = (1, 1)^T \ , \tag{6.7a}$$

$$\mathbf{w}^{S_2}_1 = (1, -1)^T \ , \tag{6.7b}$$

with $\left(\mathbf{w}^{S_1}_1\right)^T \mathbf{w}^{S_2}_1 = 0$.[13] The received signal in slot $m = 1$ and $m = 2$ is

[13] As an example, this is obtained by $S_1 = 000$ and $S_2 = 001$, c.f., Table 1.

denoted by $\mathbf{y}_{1,i}$ and $\mathbf{y}_{2,i}$ respectively. Utilizing (6.5) the received signals are given by

$$\begin{aligned}\mathbf{y}_{1,i} =& \mathbf{w}_1^{S_1}[1]\mathbf{T}_1^{S_1}\,\mathrm{Diag}\left(\bar{\mathbf{r}}\right)\mathbf{h}_{i,1} + \mathbf{w}_1^{S_2}[1]\mathbf{T}_1^{S_2}\,\mathrm{Diag}\left(\bar{\mathbf{r}}\right)\mathbf{h}_{i,2} + \mathbf{z}_{1,i}\ ,\\ \mathbf{y}_{2,i} =& \mathbf{w}_1^{S_1}[2]\mathbf{T}_1^{S_1}\,\mathrm{Diag}\left(\bar{\mathbf{r}}\right)\mathbf{h}_{i,1} + \mathbf{w}_1^{S_2}[2]\mathbf{T}_1^{S_2}\,\mathrm{Diag}\left(\bar{\mathbf{r}}\right)\mathbf{h}_{i,2} + \mathbf{z}_{2,i}\ .\end{aligned} \tag{6.8}$$

Inserting the chosen OCCs from (6.7) yields

$$\begin{aligned}\mathbf{y}_{1,i} =& \mathbf{T}_1^{S_1}\,\mathrm{Diag}\left(\bar{\mathbf{r}}\right)\mathbf{h}_{i,1} + \mathbf{T}_1^{S_2}\,\mathrm{Diag}\left(\bar{\mathbf{r}}\right)\mathbf{h}_{i,2} + \mathbf{z}_{1,i}\ ,\\ \mathbf{y}_{2,i} =& \mathbf{T}_1^{S_1}\,\mathrm{Diag}\left(\bar{\mathbf{r}}\right)\mathbf{h}_{i,1} - \mathbf{T}_1^{S_2}\,\mathrm{Diag}\left(\bar{\mathbf{r}}\right)\mathbf{h}_{i,2} + \mathbf{z}_{2,i}\ .\end{aligned} \tag{6.9}$$

The OCC are then exploited by building the sum and the difference of received signals from slots $m = 1$ and $m = 2$, which yields

$$\mathbf{y}_{1,i} + \mathbf{y}_{2,i} = 2\mathbf{T}_1^{S_1}\,\mathrm{Diag}\left(\bar{\mathbf{r}}\right)\mathbf{h}_{i,1} + \mathbf{z}_{1,i} + \mathbf{z}_{2,i}\ , \tag{6.10}$$

and

$$\mathbf{y}_{1,i} - \mathbf{y}_{2,i} = 2\mathbf{T}_1^{S_2}\,\mathrm{Diag}\left(\bar{\mathbf{r}}\right)\mathbf{h}_{i,2} + \mathbf{z}_{1,i} - \mathbf{z}_{2,i}\ . \tag{6.11}$$

A LS channel estimate is then obtained by

$$\begin{aligned}\hat{\mathbf{h}}_{i,1} &= \left(\mathbf{T}_1^{S_1}\,\mathrm{Diag}\left(\bar{\mathbf{r}}\right)\right)^H \frac{\mathbf{y}_{1,i} + \mathbf{y}_{2,i}}{2}\ ,\\ \hat{\mathbf{h}}_{i,2} &= \left(\mathbf{T}_1^{S_2}\,\mathrm{Diag}\left(\bar{\mathbf{r}}\right)\right)^H \frac{\mathbf{y}_{1,i} - \mathbf{y}_{2,i}}{2}\ .\end{aligned} \tag{6.12}$$

Please note, that (6.12) is very similar to (5.26) as the received signal, which is the sum or the difference of the received signals in (6.12), is multiplied with the conjugate transpose of the reference signal (base sequence and phase shift) as the solution to LS estimation. In the case of MU-MIMO and time domain separation however, there is no inter-user interference left in (6.12) compared to (5.26), since it was cancelled in time domain already.

The underlying assumption for this method of separation in time domain is that the channel is not changing in time between transmission of DMRS in the first slot and transmission of DMRS in the second slot, meaning approximately 500 μs. Even if this assumption is satisfied, with this method DMRS originating from only two different users can be separated, as there are only two reference signals multiplexed within one subframe and the OCC $\mathbf{w}_l^S$ is a length two sequence.

Further, please note, that I assumed the cyclic shift operator $\mathbf{T}_l^S$ as well as the base sequence $\bar{\mathbf{r}}$ in (6.6) to be independent of the slot index m, meaning they do not change within a subframe. For this, certain hopping mechanisms [10] have to be disabled.

6.3 Frequency Domain Orthogonality

Although users' channels can be separated exploiting time domain orthogonality obtained by OCCs, this method encounters severe problems as mentioned above. For MU-MIMO transmissions, orthogonality of DMRS can still be ensured in frequency domain by exploiting cyclic shift of reference symbols as in the SU-MIMO case. For this method a DMRS modification is proposed in [11] in order to obtain orthogonality not only between spatial layers of a single user but between streams originating from several UEs. This modification therefore applies on the calculation of the cyclic shift (4.5), which is substituted by

$$\tilde{n}_{\mathrm{cs},u} = \left(n_{\mathrm{cs},1} + \frac{12}{N_u}(u-1) \right) \bmod 12 \ , \tag{6.13}$$

where $n_{\mathrm{cs},1}$ is the original value of $n_{\mathrm{cs},l}$ from (4.5) for a certain CSF value and layer $l = 1$ in order to ensure backwards compatibility. For a number of users N_u that is a fraction of 12, each employing a single spatial stream, (6.13) maximizes the minimum phase shift (5.33) between users leading to good separability of frequency selective channels. In this sense, it is the ideal modification of DMRS for MU-MIMO transmissions. However, modifying phase shifts according to (6.13) is not possible in a straight forward manner, as signalling of n_{cs} is limited according to the LTE-A standard. Instead I will introduce a method of achieving DMRS orthogonality between users within the limits of the 3GPP standard.

Assigning each UE a certain value of $n_{\mathrm{cs},l}$ from (4.5), which corresponds to a certain phase shift according to (4.4), is done by means of DCI signalling. The dependence of $n_{\mathrm{cs},l}$ on the signalled CSF within the DCI is given in Table 1. As I assume each user to employ a single spatial stream, only column $l = 1$ of this table is exploited. To obtain a maximum cyclic shift between DMRS of distinct UEs, the CSF has to be selected according to a specific mapping for each user. To further investigate on such a mapping function, different numbers of users N_u are distinguished.

For $N_u \leq 4$, the CSF is chosen according to the mapping function $S = \Gamma(u)$ as given in Table 5. Comparing values of $n^{(2)}_{\mathrm{DMRS},l}$ in first row of Table 1 with the last column of Table 5, it is obvious that cyclic shifts between reference symbols of different users, in case of MU-MIMO, are identical to cyclic shifts between spatial layers, in case of SU-MIMO. This mapping from user index u to CSF S also fulfils (6.13) for $N_u = 2$ and $N_u = 4$, as is gives $n_{\mathrm{cs},l} = \{0, 6\}$ and $n_{\mathrm{cs},l} = \{0, 3, 6, 9\}$, respectively.[14] When the CSF is assigned by exploiting

[14]Please note, that the mapping in Table 5 satisfies (6.13) only in the sense that the cyclic shift between users is uniform and maximum.

Table 5: Relation between user index u and the CSF.

$\Gamma^{-1}(S)$	$\hat{\Gamma}^{-1}(S)$	CSF S	$n^{(2)}_{\mathrm{DMRS},1}$
1	1	000	0
2	4	001	6
3	7	010	3
	3	011	4
	2	100	2
	5	101	8
	6	110	10
4	8	111	9

$\Gamma(u)$, all channel estimation methods discussed in Section 5 are applicable for MU-MIMO, when the layer index l is substituted by the user index u and the number of layers N_L is substituted by the number of scheduled users N_u.

If the number of users exceeds four, i.e., $N_u > 4$, extending the mapping $\Gamma(u)$ from Table 5 to eight users is not the best choice in terms of minimum phase shift between DMRS. While the minimum difference in $n_{\mathrm{cs},1}$ between any two users is three for the mapping function $\Gamma(u)$, this minimum difference decreases to one as soon as another user is added to this mapping, cf. Table 1. Instead, a different user index to CSF mapping $\hat{\Gamma}(u)$ is exploited when $N_u > 4$ as given in Table 5. With this, the minimum difference in $n_{\mathrm{cs},1}$ between users is two for $N_u = 5, 6$ and only decreases to one for $N_u = 7, 8$. For MU-MIMO transmissions the maximum number of scheduled users N_u is eight, since the CSF within the DCI signalling is a three bit field [10]. The mapping $\hat{\Gamma}(u)$ given by Table 5 satisfies (6.13) for $N_u = 6$ in the sense that the cyclic shift between users is uniform and maximum.

6.4 Multiple Transmission Layers

When each user u is allowed to have more than just a single spatial layer, but $N_L(u)$ layers, orthogonality between DMRS has to be obtained in between spatial layers of each user and between all layers of different users simultaneously. The introduced modification (6.13) for cyclic shift values now has to be even augmented to a layer and user dependent shift as

$$\tilde{n}_{\mathrm{cs},l_u,u} = \left(n^{(1)}_{\mathrm{DMRS}} + n_{\mathrm{PN}} + \frac{12}{N^{\mathrm{tot}}_L} \left(l_u - 1 + \sum_{u'=1}^{u-1} N_L(u') \right) \right) \bmod 12 \quad (6.14)$$

with N_L^{tot} being the total number of active spatial streams

$$N_L^{\text{tot}} = \sum_{u=1}^{N_u} N_L(u) \ , \tag{6.15}$$

and the user specific layer index $l_u \in \{1, \ldots, N_L(u)\}$. The total number of layers has to be chosen as a fraction of 12 to enable maximization of cyclic shifts between layers and users. However, enforcing (6.14) by DCI signalling of a suitable CSF according to Table 1 is not straight forward. As an example, for $N_u = 2$ with $N_L(u) = 2 \ \forall u = \{1, 2\}$, the best choice is $S_1 = 000$ and $S_2 = 111$, c.f., Table 1. This results in a cyclic shift of $\Delta\alpha = \pi/2$ between any two layers, which is the maximum value for a total number of $N_L^{\text{tot}} = 4$ as already listed in Table 2. Similarly, optimal CSF values have to be found for other number of users and layers.

6.5 Simulation Results

Again computer simulations were carried out with the LTE-A Uplink Link Level Simulator [1, 42, 43] with simulation parameters as listed in Table 6. As explained previously, by applying a user to CSF mapping, estimation methods as explained in Section 5 are applicable for MU-MIMO transmissions as well. Therefore I will not show simulation results for all presented estimators again in this section, as results will show the same behaviour and properties as for SU-MIMO.

Table 6: Simulation parameters.

Parameter	Value
Simulated Subframes	4000
Channel Model	TU
Time-Fading Model	Block-Fading
Bandwidth	1.4 MHz ($N_{\text{SC}} = 72$)
Symbol Alphabet	16QAM
Antenna Configurations	4×4 (SU-MIMO)
	1×4 (MU-MIMO)
Receiver	MMSE
CE Method	sliding averaging

For verification, I show simulation results in terms of MSE for SU-MIMO with $N_T = N_L = N_R = 4$ and MU-MIMO with $N_u = N_R = 4$ in Fig. 16. As expected, results for SU-MIMO and MU-MIMO perfectly overlap when

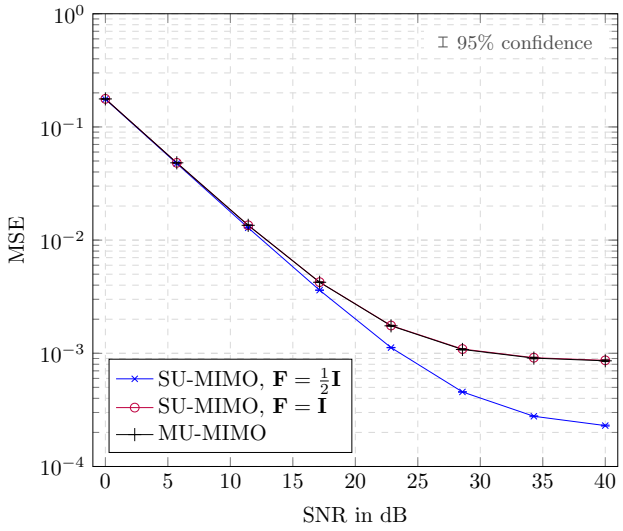

Figure 16: Channel estimation comparison for MU-MIMO.

the precoder is chosen as the identity matrix, i.e., $\mathbf{F} = \mathbf{I}$. For a standard compliant precoder from the LTE-A uplink codebook [10], which is given by $\mathbf{F} = \frac{1}{2}\mathbf{I}$ for $N_T = N_L = 4$, a difference in MSE floor at high SNR occurs, as I will explain in more detail later in this section. What is more struggling about the results shown in Fig. 16 is the fact that the estimation error seems to be independent on the squared precoder's Frobenius norm, i.e., trace $\left(\mathbf{F}^H\mathbf{F}\right)$, over a wide range of SNR. I explain this effect in more detail presently.

In case of MU-MIMO transmissions, only estimation of the effective channel, meaning actual channel and precoder, is possible exploiting DMRS, as these pilot symbols are multiplexed prior to precoding, c.f., Fig. 2. On the receive side, the actual channel cannot be calculated from the estimated effective channel in general, not even when the employed precoding matrix is perfectly known, because the dimension of the effective channel is reduced by the precoder if $N_L < N_T$. It is therefore not possible to calculate an average estimation error other than the MSE of the effective channel, which includes the precoder. Since the precoding matrix $\mathbf{F}$ is considered as part of the estimated effective channel, also the precoder scaling is part of the channel. When calculating the MSE, this scaling does actually not influence the estimation error.

Thinking of trace $\left(\mathbf{F}^H\mathbf{F}\right)$ as a transmit power then leads to the unphysical interpretation of results shown in Fig. 16, i.e., transmitting pilot symbols with higher power, also referred to as pilot boosting, does not lead to a smaller channel estimation error. In the context of estimation of the effective channel however, this power definition does not make sense but just leads to a scaling

of the channel. Instead, pilot boosting has to be accounted for in the DMRS itself.

To explain the effect of a precoder dependent error floor at high SNR, the estimation error is further analysed. Defining the estimation error vector $\boldsymbol{\varepsilon}_{i,l} = \mathbf{h}_{i,l} - \hat{\mathbf{h}}_{i,l}$ and the linear estimator $\mathbf{A}$ which is applied on the initial estimate $\tilde{\mathbf{h}}_{i,l}$, which is the sliding averaging method in case of Fig. 16, the MSE is mainly determined by

$$\begin{aligned}\boldsymbol{\varepsilon}_{i,l} =& \mathbf{h}_{i,l} - \hat{\mathbf{h}}_{i,l} \\ =& \mathbf{h}_{i,l} - \mathbf{A}\tilde{\mathbf{h}}_{i,l} \\ =& \mathbf{h}_{i,l} - \mathbf{A}\mathbf{h}_{i,l} - \mathbf{A}\sum_{\substack{p=1 \\ p\neq l}}^{N_L} \mathbf{R}_l^H \mathbf{R}_p \mathbf{h}_{i,p} - \mathbf{A}\mathbf{R}_l^H \mathbf{z}_i \ , \end{aligned} \tag{6.16}$$

where $\hat{\mathbf{h}}_{i,l} = \mathbf{A}\tilde{\mathbf{h}}_{i,l}$ and (5.27) was inserted for $\tilde{\mathbf{h}}_{i,l}$. Considering the high SNR region, i.e., $\mathbf{A}\mathbf{R}_l^H \mathbf{z}_i \approx \mathbf{0}$, the MSE is determined by two effects. When the channel is not sufficiently frequency flat, first, the term $\mathbf{h}_{i,l} - \mathbf{A}\mathbf{h}_{i,l}$ does not vanish and second, the interference term is not completely cancelled. This causes the MSE floor in Fig. 16. Since $\mathbf{h}_{i,l}$ is actually the effective MIMO channel component including the precoder $\mathbf{F}$, the precoder directly affects the residual error term at high SNR. While standard compliant precoders from the codebook are semi-unitary, i.e., trace $\left(\mathbf{F}^H\mathbf{F}\right) = 1$, exploiting the identity matrix as precoder results trace $\left(\mathbf{F}^H\mathbf{F}\right) = N_L$, similar to the MU-MIMO case, and therefore in a higher error floor.

Another difference from MU-MIMO to SU-MIMO is the maximum number of users or layers. In the LTE-A uplink up to for spatial layers are exploited for SU-MIMO transmissions, leading to a minimal cyclic shift of $\Delta\alpha_{\min} = \frac{\pi}{2}$ between MIMO channels. For MU-MIMO the number of users is limited by the number of CSF and a corresponding mapping between users and CSF values, as shown in Table 5, leading to a maximum of $N_u = 8$. In this case the minimum cyclic shift in between user channels is $\Delta\alpha_{\min} = \frac{\pi}{6}$. Separation of user channels is therefore only possible for channels of low RMS delay spread, or differently, only few users should be scheduled on channels with high delay spread.

To emphasize this relation, simulations of MU-MIMO transmissions with $N_u = \{1, 2, 4, 6, 8\}$ and $N_R = 8$ were carried out on a TU channel. For channel estimation, sliding averaging with $\bar{\gamma} = \{1, 2, 4, 6, 8\}$ for $N_u = \{1, 2, 4, 6, 8\}$ users was chosen, respectively. Simulation results in Fig. 17 obviously show the previously explained effect. As the number of users grows, on a channel with moderate RMS delay spread, the MSE floor at high SNR rises, as shown

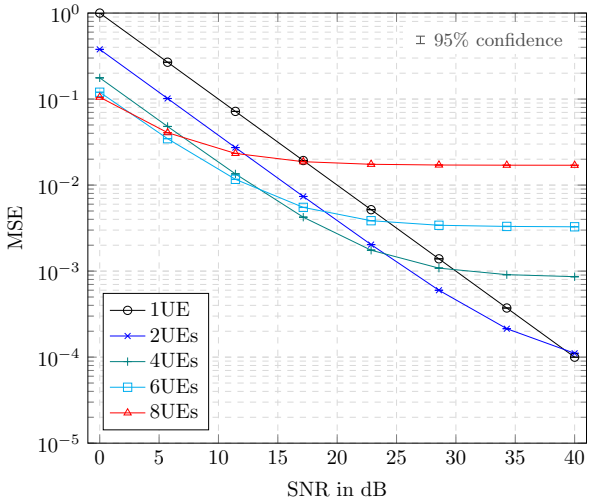

(a) User MSE.

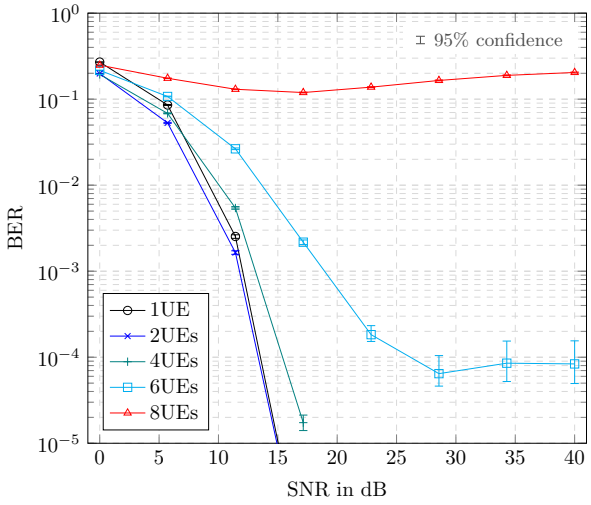

(b) Uncoded BER for 16QAM.

Figure 17: MU-MIMO channel estimation comparison for different number of users.

in Fig. 17a. The resulting BER, as shown in Fig. 17b, reveals the effect of receive diversity. As the number of receive antennas is fixed to $N_R = 8$, an essential SNR gain is achieved when less than 8 users are transmitting. Results show that in the case of $N_u = 6$ a very low residual BER is reached due to receive diversity, even when the MSE floor appears high compared to cases with less users.

Still, for $N_u = 6$ the residual MSE at low noise is already quite high. Therefore, a high number of users, such as $N_u = 6$ or $N_u = 8$ is only applicable on a channel with low RMS delay spread, as the user separation has to be seen in relation to frequency selectivity. While $N_u = 8$ does not lead to a vanishing BER on the TU channel, 8 users are likely separable on a PedA channel. On the other hand, a number of users $N_u = 6$ leads to very low BER at high SNR in this specific example while it will most likely lead to very high BER on a more frequency selective channel such as the VehB.

7 Channel Interpolation

So far, several methods of channel estimation were introduced and discussed. All of them aim to obtain channel estimates at pilot symbol positions. For demodulation and detection of course the channel needs to be estimated at all time-frequency positions at which data is transmitted. Therefore the estimated channel has to be interpolated in between channel estimates.

Considering the allocation of DMRS within the time-frequency resource grid, as for example shown in Fig. 3, no interpolation in frequency domain has to be carried out as there are channel estimates available for all subcarriers already. Interpolation is only carried out in time domain for each subcarrier k and each spatial layer l (or each user u) individually. Although the dense allocation of reference symbols in frequency domain eliminated the need for frequency domain interpolation or even 2D interpolation, the loose allocation in time domain implies difficulties for channel interpolation, especially on a time variant channel. Comparing the LTE-A uplink DMRS allocation to the downlink case, as shown in Fig. 4, there are pilot symbols allocated at four different symbol times in the downlink while there are DMRS at only two symbol times in the uplink. As DMRS are multiplexed at OFDM symbol times $n = 4$ and $n = 11$ in every subframe, the channel is interpolated between channel estimates at these positions, i.e., for $n \in \{5, \ldots, 10\}$. In order to obtain the channel estimate for the whole subframe, the channel needs to be extrapolated for symbol times before the first and after the second DMRS of a subframe, i.e., for $n \in \{1, \ldots, 4, 12, \ldots, 14\}$. Further, interpolation of time variant channels is challenging with the LTE-A uplink DMRS allocation as there are only two channel estimates per subframe. Considering a single subframe, at most an interpolation function of order one, i.e., a linear function can be fit to these two points. To incorporate more points of the estimated channel in an interpolation scheme, also previous and subsequent subframes are considered in [47] in order to obtain a better fit to a time variant channel.

In this chapter I will describe different methods of channel interpolation for time variant channels. I assume the channel to be sufficiently flat in time, such that the introduced system model is still valid. To verify this assumption, the fundamental relation between coherence time T_{coh} and Doppler frequency f_D is considered. It is known [40] to be

$$T_{\text{coh}} \approx \frac{1}{f_D} \,, \tag{7.1}$$

with Doppler frequency

$$f_D = f_c \frac{v}{c_0} \,, \tag{7.2}$$

where c_0 is the speed of light, v is the user's speed and f_c is the center frequency of uplink transmission. Combining (7.1) and (7.2), assuming a center frequency of $f_c = 1.9\,\mathrm{GHz}$ and inserting LTE-A's OFDM symbol duration of approximately $71\,\mu\mathrm{s}$ as coherence time, yields a maximum user speed of

$$v = \frac{c_0}{T_{\mathrm{coh}} f_c} = \frac{3 \cdot 10^8 \,\frac{\mathrm{m}}{\mathrm{s}}}{71\,\mu\mathrm{s} \cdot 1.9\,\mathrm{GHz}} \approx 2255.6\,\frac{\mathrm{m}}{\mathrm{s}}\ . \tag{7.3}$$

This shows, that assuming the channel to be constant for the duration of an OFDM symbol is a justified assumption up to very high speeds. Of course, on a time-variant channel the system model introduced in Section 3 is only an approximation as it assumes the channel to be time constant. However, the occurring ICI is negligible, as shown in [48].

Further I consider exploiting channel estimates from previous subframes in order to fit higher order (cubic) interpolation functions for interpolation of time variant channels. As exploiting channel estimates originating from subsequent subframes inherently introduces a processing delay, I only consider the current subframe together with estimates from previous subframes. As interpolation is carried on the estimated effective channel (for SU-MIMO), considering past points is therefore only possible if the number of layers does not change in time, as this means that also channel matrix dimensions change in time. Interpolation on the actual (non-effective) channel cannot be performed, as the actual channel cannot be recovered from the effective one if $N_L < N_T$ as the precoder reduces the effective channel's dimension compared to the actual channel. For MU-MIMO the dimension of the channel is also time variant, meaning it changes from subframe to subframe, as the schedule changes with time. Considering a previous estimated channel coefficient when interpolating the channel on a certain layer (for a certain user) is only possible if this layer (user) did also exist in the previous subframe.

In order to gain from exploiting past points in channel interpolation, practically one has to assume that channel dimensions, meaning the number of spatial layers for SU-MIMO and scheduled users for MU-MIMO, to change slowly over time, i.e., to be constant for several consecutive subframes. To show possible gains, I assume the number of layers (user) to be constant in my simulations.

7.1 Methods

In this section I introduce interpolation methods of different complexity and compare their ability to fit the time-variant channel. Within this description I refer to the subframe with OFDM symbol time indices $n \in \{1, \ldots, 14\}$ as

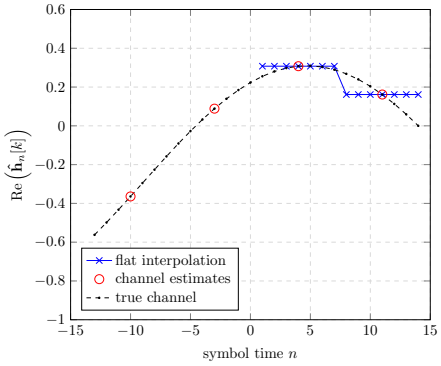

(a) Flat interpolation 2 points.

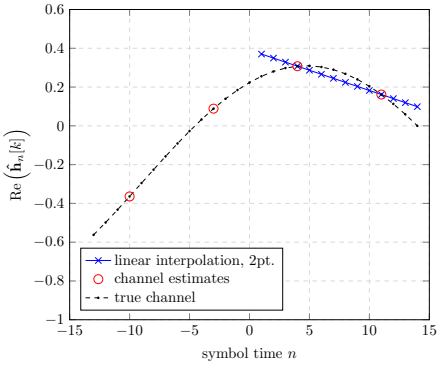

(b) Linear interpolation 2 points.

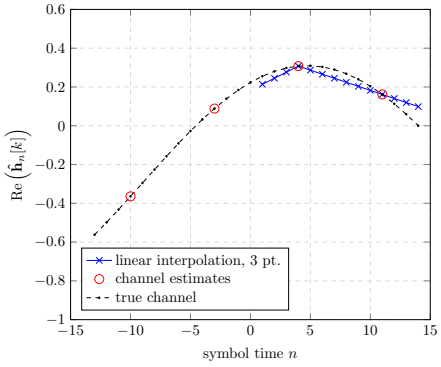

(c) Linear interpolation 3 points.

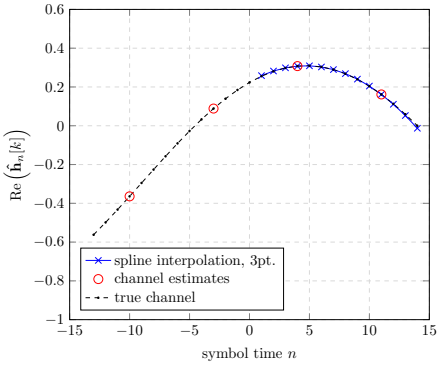

(d) Spline interpolation 3 points.

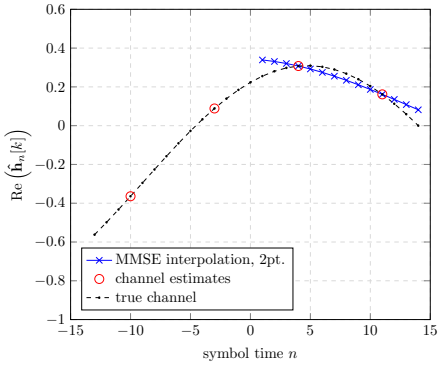

(e) DPSS interpolation 2 points.

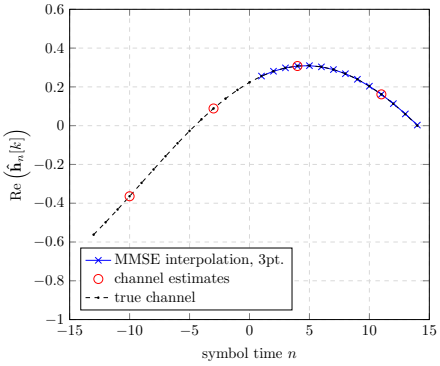

(f) DPSS interpolation 3 points.

Figure 18: Comparison of interpolation methods.

the current subframe and to the subframe with OFDM symbol time indices $n \in \{-13, \ldots, 0\}$ as the previous subframe.

7.1.1 Flat Interpolation

The easiest way to obtain channel estimates in between pilot positions is re-using the estimated channel coefficients from these positions also for all remaining time-frequency grid positions in a RB, meaning within the same slot. I refer to this method as flat interpolation as the estimated channel is constant in time for each slot as shown in Fig. 18a. It is obvious, that knowledge of channel estimates from the previous subframe does not improve this estimation method at all. This method is of very low complexity, however, it is not able to track the channel's time variation in case of high user mobility.

7.1.2 Linear Interpolation

A method of slightly higher complexity than flat interpolation is linear interpolation. In this case the interpolated channel is obtained by fitting a linear function through the channel estimates at pilot positions within a subframe, as shown in Fig. 18b. This curve fitting is actually straight forward as there are exactly two known channel estimates in a subframe. Although linear interpolation is able to describe channel variations in time for a slowly fading channel, approximating a rapidly time-variant channel with a linear function leads to high estimation errors in general. As one observes in Fig. 18b, the linear interpolation differs from the true channel significantly, especially for symbol times lying not in between the pilot positions. In order to reduce this effect, the estimated channel coefficient from the second slot of the previous subframe is considered in the linear interpolation, which now includes three estimated points. In this case the interpolated channel between DMRS positions of the current subframe are obtained as before, whereas the interpolated channel for $n \in \{1, 2, 3\}$ is obtained by fitting a linear function from the estimated channel of the second slot in the previous subframe ($n = -3$) to the estimated channel in the first slot of the current subframe ($n = 4$), as shown in Fig. 18c. It is obvious, that including further channel estimates from previous subframes does not have an impact on the interpolated channel of the current subframe.

7.1.3 Spline Interpolation

In order to obtain an interpolated channel that is not piecewise flat or approximates the time-variant channel by piecewise linear functions, higher order interpolation functions have to be exploited. In this sense, a very

common method for interpolation is cubic spline interpolation, to which I will refer just as spline interpolation in this work. This methods aims to fit pieces (splines) of cubic polynomials to the estimated channel values obtaining a two times continuously differentiable function [49].

Since this method is implemented by the MATLAB build in function *interp1* [50], spline interpolation automatically degenerates to linear interpolation when only two points of the estimated channel are considered. In order to fit a cubic interpolation function to the estimated channel, at least three points are required for interpolation. As MATLAB employs so called not-a-knot boundary conditions for spline interpolation, a single cubic interpolation function is fit through three sample points. However, this is not considered a cubic spline interpolation since in this special case only a single cubic function is utilized instead of actual cubic splines. To obtain a real cubic spline interpolation in this sense, at least four sample points are required.

By including also channel estimates from previous subframes into spline estimation, higher order polynomials are fit through the estimated channel, as shown in Fig. 18d. In this case, a time-varying channel is interpolated by a smooth function leading to decreased channel estimation error compared to flat and linear interpolation.

7.1.4 Interpolation using DPSS

Basis expansion models are commonly exploited for estimation of frequency selective channels [51]. Dependent on the basis, these methods lead to channel estimates that are not only linear functions in time, as for example with linear interpolation, also when only two sample points are available. In [52] authors consider Discrete Prolate Spheroidal Sequence (DPSS) for estimation of time-variant channels. As DPSS are orthogonal over a finite set as well as on an infinite set making them especially suited for CE because there is no windowing necessary as for example with Fourier basis aided estimation. They are sequences which are band limited in $[-\nu_{\mathrm{D}}, \nu_{\mathrm{D}}]$ and simultaneously most concentrated in time, as found by Slepian in [53]. The set of time indices in this context is given by an LTE-A subframe, i.e., $n \in \{1, \ldots, 14\}$. Here ν_{D} denotes the normalized Doppler frequency and is given by

$$\nu_{\mathrm{D}} = f_D T_s \ , \tag{7.4}$$

where T_s is the OFDM symbol duration and f_D is the Doppler frequency from (7.2). The index limited DPSS are denoted by $\mathbf{u}_j \in \mathbb{R}^{14\times 1}$ and defined as eigenvectors of matrix $\mathbf{V} \in \mathbb{R}^{14\times 14}$, fulfilling

$$\mathbf{V}\mathbf{u}_j = \lambda_j \mathbf{u}_j \ , \tag{7.5}$$

with

$$\mathbf{V}[k,l] = \frac{\sin(2\pi((k-1)-(l-1)))\nu_{\mathrm{Dmax}}}{\pi((k-1)-(l-1))} \qquad k,l \in \{1,\ldots,14\} \ . \tag{7.6}$$

The interpolated channel is then obtained by basis expansion

$$\hat{\mathbf{h}}_{n,i,l}[k] = \sum_{k=0}^{D-1} \mathbf{u}_j[n]\boldsymbol{\rho}[j] \qquad i \in \{1,\ldots,N_R\}, l \in \{1,\ldots,N_L\} \ , \tag{7.7}$$

with the signal space dimension D. From this description it is obvious that the basis depends on the user speed v as well as on the subframe length.

In [52] authors describe that the eigenvalues λ_i decrease rapidly such that the signal space dimension D can be chosen small compared to the number of sample points (pilot positions). As there are only two reference symbols per subframe in the LTE-A uplink, I chose the signal space dimension equal to the number of pilot positions, e.g., $D = 2$, for a *2 point* DPSS interpolation.

Defining the vector

$$\mathbf{f}_n = \begin{pmatrix} \mathbf{u}_0[m] \\ \vdots \\ \mathbf{u}_{D-1}[m] \end{pmatrix} \ , \tag{7.8}$$

and the correlation matrix

$$\mathbf{C}_f = \sum_{n\in\{4,11\}} \mathbf{f}_n \mathbf{f}_n^H \ , \tag{7.9}$$

the basis expansion parameters $\hat{\boldsymbol{\rho}} = (\hat{\boldsymbol{\rho}}[0]\ldots,\hat{\boldsymbol{\rho}}[D-1])^T$ are estimated (according to [52]) as

$$\hat{\boldsymbol{\rho}} = \mathbf{C}_f^{-1} \sum_{n\in\{4,11\}} \hat{\mathbf{h}}_n[k]\mathbf{f}_n^{\star} \ . \tag{7.10}$$

7.1.5 2D MMSE Estimation

As a performance reference a 2D MMSE estimator of window size two is introduced, meaning the channel is estimated on all time-frequency positions at once. In order to enable for description of channel correlations by correlation matrices, the stacked channel vectors $\underline{\mathbf{h}}_{n,i}$ at OFDM symbol time n from (5.5) are again stacked to include all symbol times $n \in \{1,...,14\}$ into vector

$$\bar{\mathbf{h}}_i = \begin{pmatrix} \underline{\mathbf{h}}_{1,i} \\ \underline{\mathbf{h}}_{2,i} \\ \vdots \\ \underline{\mathbf{h}}_{14,i} \end{pmatrix} \in \mathbb{C}^{14N_{\mathrm{SC}}N_L\times 1} \ . \tag{7.11}$$

Defining the channel vector at the reference symbol positions to be

$$\bar{\mathbf{h}}_i^{\mathcal{R}} = \begin{pmatrix} \underline{\mathbf{h}}_{4,i} \\ \underline{\mathbf{h}}_{11,i} \end{pmatrix} \in \mathbb{C}^{2N_{\mathrm{SC}}N_L \times 1} \ , \tag{7.12}$$

and similarly including reference symbols $\underline{\mathbf{R}}_n$ of OFDM symbol time $n = \{4, 11\}$ into a matrix

$$\bar{\mathbf{R}} = \begin{pmatrix} \underline{\mathbf{R}}_4 & \\ & \underline{\mathbf{R}}_{11} \end{pmatrix} \in \mathbb{C}^{2N_{\mathrm{SC}} \times 2N_{\mathrm{SC}}N_L} \ , \tag{7.13}$$

the received signal at receive antenna i in terms of a vectorized system model is given by

$$\bar{\mathbf{y}}_i = \begin{pmatrix} \mathbf{y}_{4,i} \\ \mathbf{y}_{11,i} \end{pmatrix} = \bar{\mathbf{R}}\bar{\mathbf{h}}_i^{\mathcal{R}} + \bar{\mathbf{z}}_i \ . \tag{7.14}$$

Similar to Appendix A.2 the MMSE estimator is then given by

$$\mathbf{A}^{\mathrm{LMMSE}} = \mathbf{C}_{\bar{\mathbf{h}}\bar{\mathbf{y}}}\mathbf{C}_{\bar{\mathbf{y}}}^{-1} \ , \tag{7.15}$$

with correlation matrices $\mathbf{C}_{\bar{\mathbf{y}}} \in \mathbb{C}^{2N_{\mathrm{SC}} \times 2N_{\mathrm{SC}}}$ and $\mathbf{C}_{\bar{\mathbf{h}}\bar{\mathbf{y}}} \in \mathbb{C}^{14N_{\mathrm{SC}}N_L \times 2N_{\mathrm{SC}}}$ given by

$$\begin{aligned} \mathbf{C}_{\bar{\mathbf{y}}} =& \mathbb{E}\{\bar{\mathbf{y}}\bar{\mathbf{y}}^H\} \\ =& \mathbb{E}\left\{ \left(\bar{\mathbf{R}}\bar{\mathbf{h}}^{\mathcal{R}} + \bar{\mathbf{z}}\right) \left(\bar{\mathbf{R}}\bar{\mathbf{h}}^{\mathcal{R}} + \bar{\mathbf{z}}\right)^H \right\} \\ =& \bar{\mathbf{R}}\mathbf{C}_{\bar{\mathbf{h}}^{\mathcal{R}}}\bar{\mathbf{R}}^H + \sigma_{\mathbf{z}}^2\mathbf{I}_{2N_{\mathrm{SC}}} \ , \end{aligned} \tag{7.16}$$

and

$$\begin{aligned} \mathbf{C}_{\bar{\mathbf{h}}\bar{\mathbf{y}}} =& \mathbb{E}\left\{\bar{\mathbf{h}}\bar{\mathbf{y}}^H\right\} \\ =& \mathbb{E}\left\{\bar{\mathbf{h}}\left(\bar{\mathbf{R}}\bar{\mathbf{h}}^{\mathcal{R}} + \bar{\mathbf{z}}\right)^H\right\} \\ =& \mathbf{C}_{\bar{\mathbf{h}}\bar{\mathbf{h}}^{\mathcal{R}}}\bar{\mathbf{R}}^H \ . \end{aligned} \tag{7.17}$$

Similar to (5.14) the correlation matrices can be written in terms of Kronecker products as the channel is vectorized

$$\mathbf{C}_{\bar{\mathbf{h}}^{\mathcal{R}}} = \mathbf{C}_{\mathbf{h}^{\mathcal{R}}}^{(t)} \otimes \mathbf{C}_{\mathbf{h}}^{(s)} \otimes \mathbf{C}_{\mathbf{h}}^{(f)} \ , \tag{7.18}$$

with the channel time auto-correlation matrix $\mathbf{C}_{\mathbf{h}^{\mathcal{R}}}^{(t)} \in \mathbb{C}^{2\times 2}$ describing the channel correlation at symbol times where reference symbols are multiplexed, i.e., $n = \{4, 11\}$. Similarly

$$\mathbf{C}_{\bar{\mathbf{h}}\bar{\mathbf{h}}^{\mathcal{R}}} = \mathbf{C}_{\mathbf{h}\mathbf{h}^{\mathcal{R}}}^{(t)} \otimes \mathbf{C}_{\mathbf{h}}^{(s)} \otimes \mathbf{C}_{\mathbf{h}}^{(f)} \ , \tag{7.19}$$

with the channel time cross-correlation matrix $\mathbf{C}^{(t)}_{\mathbf{hh}^{\mathcal{R}}} \in \mathbb{C}^{14\times 2}$ describing the channel correlation between symbol times of reference symbols, i.e., $n = \{4, 11\}$, and all other symbol times $n = \{1, \ldots, 14\}$ as in [54].

Although the MMSE estimator is described for a window size of two, meaning two reference symbols of the current subframe, it extends easily by including the channel of previous subframes in (7.11) and (7.12) and modifying all reference symbol and correlation matrices accordingly. In this way, a 2D MMSE estimator for arbitrary window sizes is obtained.

7.2 Simulation Results

As previously, simulations were carried out employing the Vienna LTE-A Uplink Link Level Simulator [1, 42, 43]. Main simulation parameters are listed in Table 7. To obtain a doubly-selective channel, the channel is generated time variant according to [55], where fast-fading means, the channel is changing even within an OFDM symbol. To investigate performance of introduced interpolation methods, channel estimates at pilot positions are obtained by MMSE estimation according to Section 5.2. Further, I assume the number of layers to be fixed to $N_L = 2$, such that the effective channels' dimension is constant for all subframes. This allows considering channel estimates obtained in previous subframes.

Simulation results of the 2D MMSE estimator serve as performance reference. Although this seems unfair in terms of comparison since all other schemes are 1D, performance of 2×1D MMSE estimation is virtually the same as 2D MMSE estimation [56].

Simulation results are shown in Fig. 19 in terms of MSE over user velocity v. Figure 19a and Fig. 19b show results obtained by considering the current subframe only, meaning two channel estimates, at low and high SNR, respectively. Similarly, Fig. 19c and Fig. 19d show results obtained when an additional channel estimate from the previous subframe is taken into account for interpolation, for low and high SNR, respectively. In any case, the MSE of 2D MMSE interpolation for a certain number of points is shown, where the number of sample points corresponds to the window size of MMSE estimation.

As one would expect, flat interpolation, as the interpolation method of lowest complexity, shows a severe performance gap to all other interpolation schemes. Even at low user speeds, this method is not able to track the time variant channel which leads to increased MSE. Only at a very low SNR for very low velocities, flat interpolation is superior to linear and spline interpolation. Fitting the time variant channel fails at low SNR when linear or spline interpolation is applied as rather the noise than the actual channel is fit by the interpolating function.

Linear interpolation shows good performance at low velocity but gets worse at higher speeds as this method cannot describe time variations of the channel accurately. When three sample points of channel estimates are considered, linear interpolation even outperforms cubic spline interpolation at low SNR. Although in the linear as in the spline case, the noise has a significant impact on the interpolation, cubic spline interpolation seems to suffer even more from this effect.

In a high SNR region, spline interpolation performs better than linear interpolation in terms of MSE for a wide range of user velocity. At user speeds above approximately 300 km/h however, there is no more gain of spline interpolation over *3pt. linear*. When the channel is rapidly varying with time, neither *3pt. linear* nor *3pt. spline* interpolation is able to fit the channel coefficients and both result in a very high estimation MSE.

Interpolation exploiting DPSS, which I will refer to simply as DPSS interpolation, shows a very impressive overall MSE performance. Since these basis functions are obtained by an eigenvalue decomposition where eigenvalues rapidly decay, the basis expansion requires only very few coefficients. This means, that the interpolation based on basis expansion is able to describe the time-variant nature of the channel with a very limited number of sample points. DPSS interpolation is therefore very close to the MMSE performance. However, one has to keep in mind, that calculating the basis functions requires knowledge of the exact user speed, which is assumed to be perfectly known in my simulation.

Table 7: Simulation parameters.

Parameter	Value
Simulated Subframes	1000
Channel Model	TU
Time-Fading Model	Fast-Fading
User Velocity	$5 - 400\,\mathrm{km/h}$
Bandwidth	$1.4\,\mathrm{MHz}$ ($N_{\mathrm{SC}} = 72$)
Antenna Configurations	2×2, $N_L = 2$
CE Method	MMSE

Another comparison of estimation MSE for different numbers of exploited sample points is shown in Fig. 20, where Fig. 20a shows results for low SNR and Fig. 20b shows results for high SNR, respectively. Results show that it is not necessarily beneficial to exploit more points for interpolation in general. While *3pt. linear* clearly performs better than *2pt. linear*, exploiting more than two points also decreases MSE for DPSS interpolation at high speeds.

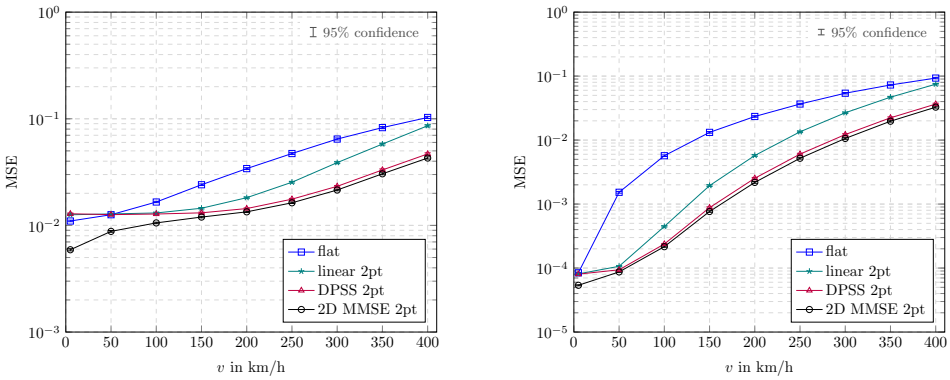

(a) SNR=7dB, 2 points.

(b) SNR=30dB, 2 points.

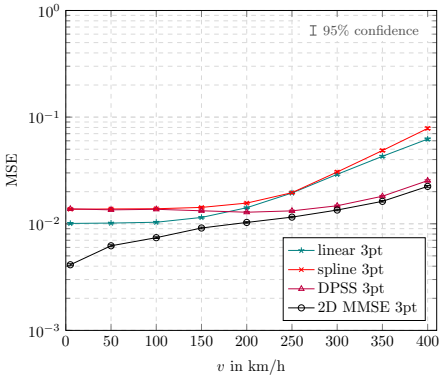

(c) SNR=7dB, 3 points.

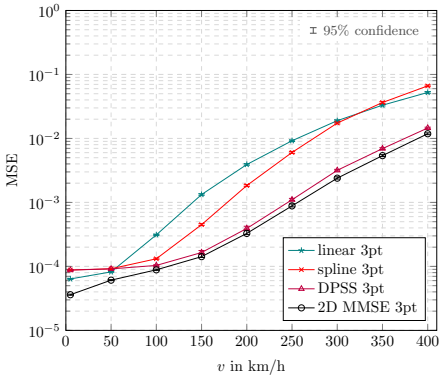

(d) SNR=30dB, 3 points.

Figure 19: Comparison of interpolation methods.

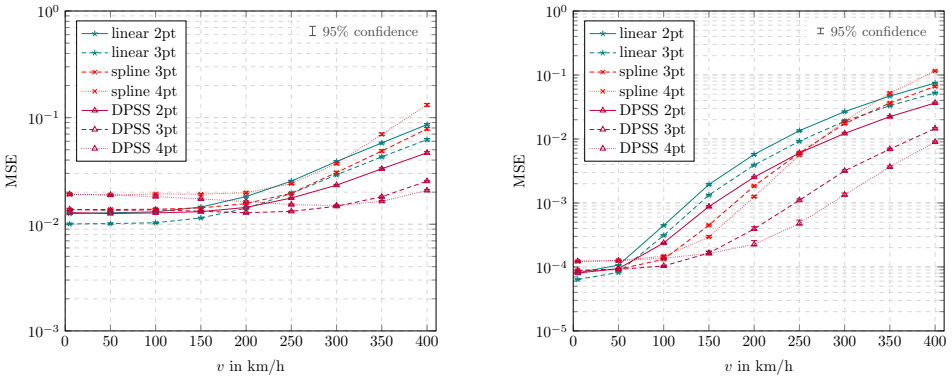

(a) SNR=7dB. (b) SNR=30dB.

Figure 20: Comparison of interpolation methods for different number of sample points.

This is however not true for spline interpolation. At low and at high SNR, *3pt. spline* shows higher MSE than *2pt. spline* at high velocities. Although *3pt. spline* outperforms *2pt. spline* in certain speed ranges, considering an additional point does not seem to pay of with cubic spline interpolation in general. This is contrary to DPSS, where adding channel estimation sample points also decreases the estimation MSE at high speed. At low speed however, both, DPSS and spline, loose against linear interpolation. In this region of operation these methods try to fit a channel variation that is actually not present. Instead the high noise contribution leads to a wrong interpolation result. Again, here this effect is more dominant than with linear interpolation.

8 Conclusion

In my work I consider the problem of doubly selective channel estimation for LTE-A uplink transmissions. A major difference in the pilot based channel estimation from downlink to uplink transmissions is the special way of multiplexing DMRS with the data. In order to reduce overhead for uplink MIMO transmissions, reference symbols are multiplexed on the same time-frequency positions for all spatial streams, originating from one or more users. Another big difference is, that SC-FDM is employed as physical layer access scheme in the uplink while OFDM is employed in the downlink. Although this has major impacts on system performance, in terms of throughput and BER, challenges in CE occur due to the special pilot allocation pattern rather than due to the single-carrier character of uplink transmissions.

Fur the purpose of MIMO CE, all MIMO channels need to be separated at the receiver. For this reason, code-domain orthogonality of DMRS is exploited. Many common methods from literature transform the received pilot symbols in frequency domain and then separate CIRs by windowing, which is referred to as DFT based estimation. For channels with a certain frequency selectivity, which corresponds to a long CIR, these methods suffer from CIR leakage. This means that CIRs are too long and actually overlap in time domain. It is therefore not possible to apply simple windowing.

Concluding from this, separability of MIMO CIRs depends on the number of MIMO channel components, meaning either the number of spatial layers in SU-MIMO or the number of users in MU-MIMO, and on the frequency selectivity of the channel. If either of these figures of merit is high, the channel components cannot be separated at the receiver sufficiently well. In this context, the minimum cyclic shift between spatial layers $\Delta\alpha_{\min}$ is a direct measure of distance between MIMO channel components and therefore highly related to separability.

Separating all MIMO channel components is equivalent to estimating a desired MIMO channel, from a certain layer to a certain receive antenna, and cancelling the inter-layer interference, originating from DMRS of all other MIMO channel components. I introduce two LS based CE methods that aim to cancel this interference entirely in frequency domain. Both methods, namely sliding averaging and quadratic smoothing, apply post-processing on an initial estimate obtained by LS estimation. While the initial estimate is not suited for demodulation purposes as it contains severe inter-layer interference, both methods cancel inter-layer interference sufficiently, such that a channel estimate suitable for demodulation is obtained. Although these schemes do not separate CIRs in time domain and therefore do not suffer from CIR leakage, inter-layer interference cancellation is more challenging if the

channel has a higher delay spread. As the DMRS code-domain orthogonality is destroyed when transmitted over a frequency selective channel, interference cancellation is deteriorated. Still, proposed CE methods achieve lower estimation MSE than conventional DFT based estimation methods over wide ranges of SNR, especially when a narrow transmission band is employed. This means, proposed CE methods show superior separation capabilities compared to DFT based estimation algorithms.

QS estimation shows a quite high error floor at high SNR and sliding averaging estimation results in a very poor performance at low SNR. Contrary, QS estimation performs well at low SNR while sliding averaging has a much worse MSE in that SNR region. As a further step in terms of CE, a smoothing that consists of a convex weighting of these two post-processing schemes can be applied on the initial estimate. Making the convex weighting SNR dependent will lead to a estimation method that shows good performance in the whole SNR region of interest.

Further I show that MU-MIMO and SU-MIMO operations are very similar in terms of uplink. Besides the precoding matrix, there is virtually no change in the transmission model from the SU to the MU case. For CE however, certain implications with respect to the DMRS structure have to be considered. While for SU-MIMO, code-domain orthogonality is obtained by cyclic shifts between several transmission layers of a single user, for MU-MIMO orthogonality has to be obtained by cyclic shifts in between spatial streams from several different users. This has to be ensured by means of signalling. Although some authors consider the problem of CE in the context of LTE-A uplink MU-MIMO, literature does not provide a clear strategy for choosing cyclic shifts such that channels originating from different users are separable. I introduce a way of signalling cyclic shift values to users such that code-domain orthogonality is obtained similar to the SU-MIMO case. With this proposed mapping between users and cyclic shift values, all introduced estimation methods are applicable in the MU case as well.

To obtain channel estimates at time-frequency positions where no pilot symbols are multiplexed, interpolation in between these positions is performed. Since the reference symbol allocation is as dense as possible in frequency domain, meaning there are pilot symbols on every subcarrier, interpolation is only carried out in time domain. When the channel to be estimated is time-selective, this implies difficulties. As there are only two symbol time indices where DMRS are scheduled, there are only two channel estimates available for interpolation within a subframe. Without any other prior knowledge about the channel, this naturally only allows for linear interpolation between these two estimates. For a fast time-varying channel, this interpolation scheme is obviously not capable of describing the channel's time variations.

In my work I consider and compare various interpolation methods that aim to interpolate a time-variant channel sufficiently well. A first option to improve interpolation performance is to take more than two channel estimates into account for interpolation. While requiring storing of previous channel estimates, this allows to fit splines between sample points. When one previous channel estimate is considered, meaning three points in total, linear splines can be fitted. When at least two previous estimates are taken into account, cubic splines can be exploited for interpolation.

As a second option for improving interpolation, a basis expansion model of suited basis functions is exploited. For this purpose I chose DPSS for interpolation in my work. Although these basis functions are capable of describing channel variations over time very accurately, they already depend on the actual user velocity. A prior knowledge about the user speed is therefore necessary to apply this interpolation method.

I show by simulations that the choice of interpolation scheme has minor effect on the estimation MSE at low speeds, meaning less than 50 km/h at a carrier frequency of $f_c = 1.9\,\text{GHz}$. For low SNR, higher complexity of spline interpolation does not pay off compared to linear interpolation. Even at very high SNR, taking into account more points with spline interpolation reduces estimation errors only in a certain velocity range.

Interpolation with a DPSS basis expansion achieves low estimation MSE in general. This superior performance however, comes at the cost of prior knowledge of user speed. For a practical implementation in a mobile communication system this prior knowledge of course needs to be estimated. A further investigation of the influence on estimation errors of user velocity on the channel estimation error is therefore an interesting research question.

A Appendix

A.1 Circulant Matrices

A circulant matrix

$$\mathbf{C} = \begin{pmatrix} c_0 & c_{N-1} & \dots & c_2 & c_1 \\ c_1 & c_0 & c_{N-1} & & c_2 \\ \vdots & c_1 & c_0 & \ddots & \vdots \\ c_{N-2} & & \ddots & \ddots & c_{N-1} \\ c_{N-1} & c_{N-2} & \dots & c_1 & c_0 \end{pmatrix} \in \mathbb{C}^{N\times N} \tag{A.1}$$

that is fully described by its first column vector $\mathbf{c} = (c_0, c_1, \dots, c_{N-1})^T \in \mathbb{C}^{N\times 1}$ gets diagonalized by applying the unitary DFT $\mathbf{D}_N \in \mathbb{C}^{N\times N}$

$$\mathbf{C} = \mathbf{D}_N^H \operatorname{Diag}(\mathbf{D}_N \mathbf{c})\, \mathbf{D}_N \ . \tag{A.2}$$

Applying this theorem on the block-wise circulant channel matrix (3.5), that can be written as

$$\mathbf{H}^{(\text{circ})} = \begin{pmatrix} \mathbf{H}_{1,1}^{(\text{circ})} & \dots & \mathbf{H}_{1,N_T}^{(\text{circ})} \\ \vdots & \ddots & \vdots \\ \mathbf{H}_{N_R,1}^{(\text{circ})} & \dots & \mathbf{H}_{N_R,N_T}^{(\text{circ})} \end{pmatrix} \ , \tag{A.3}$$

leads to the block wise diagonal channel matrix (3.6)

$$\mathbf{H}^{(\text{diag})} = \begin{pmatrix} \mathbf{D}_{N_{\text{FFT}}} \mathbf{H}_{1,1}^{(\text{circ})} \mathbf{D}_{N_{\text{FFT}}}^H & \dots & \mathbf{D}_{N_{\text{FFT}}} \mathbf{H}_{1,N_T}^{(\text{circ})} \mathbf{D}_{N_{\text{FFT}}}^H \\ \vdots & \ddots & \vdots \\ \mathbf{D}_{N_{\text{FFT}}} \mathbf{H}_{N_R,1}^{(\text{circ})} \mathbf{D}_{N_{\text{FFT}}}^H & \dots & \mathbf{D}_{N_{\text{FFT}}} \mathbf{H}_{N_R,N_T}^{(\text{circ})} \mathbf{D}_{N_{\text{FFT}}}^H \end{pmatrix} \tag{A.4}$$

$$= \begin{pmatrix} \operatorname{Diag}\left(\mathbf{D}_{N_{\text{FFT}}} \bar{\mathbf{h}}_{1,1}\right) & \dots & \operatorname{Diag}\left(\mathbf{D}_{N_{\text{FFT}}} \bar{\mathbf{h}}_{1,N_T}\right) \\ \vdots & \ddots & \vdots \\ \operatorname{Diag}\left(\mathbf{D}_{N_{\text{FFT}}} \bar{\mathbf{h}}_{N_R,1}\right) & \dots & \operatorname{Diag}\left(\mathbf{D}_{N_{\text{FFT}}} \bar{\mathbf{h}}_{N_R,N_T}\right) \end{pmatrix} \tag{A.5}$$

where (A.2) was exploited.

A.2 The Minimum Mean Square Error Estimator

From the received signal

$$\mathbf{y} = \mathbf{R}\mathbf{h} + \mathbf{z} \ , \tag{A.6}$$

with noise $\mathbf{z} \sim \mathcal{CN}(\mathbf{0}, \sigma_{\mathbf{z}}^2 \mathbf{I}_{N_{\mathrm{SC}}})$, the channel vector $\mathbf{h}$ is estimated exploiting the linear estimator $\mathbf{A}$ as

$$\hat{\mathbf{h}} = \mathbf{A}\mathbf{y} \ . \tag{A.7}$$

To obtain the LMMSE estimator, the mean squared error has to be minimized, leading to

$$\begin{aligned}
\mathbf{A}^{\mathrm{LMMSE}} &= \arg\min_{\mathbf{A}} \mathbb{E}\left\{ \left\| \mathbf{A}\mathbf{y} - \mathbf{h} \right\|_2^2 \right\} \\
&= \arg\min_{\mathbf{A}} \mathbb{E}\left\{ (\mathbf{A}\mathbf{y} - \mathbf{h})^H (\mathbf{A}\mathbf{y} - \mathbf{h}) \right\} \\
&= \arg\min_{\mathbf{A}} \mathbb{E}\left\{ \mathrm{trace}\left\{ (\mathbf{A}\mathbf{y} - \mathbf{h}) (\mathbf{A}\mathbf{y} - \mathbf{h})^H \right\} \right\} \\
&= \arg\min_{\mathbf{A}} \mathrm{trace}\left\{ \mathbf{A}\mathbf{C}_{\mathbf{y}}\mathbf{A}^H - \mathbf{C}_{\mathbf{hy}}\mathbf{A}^H - \mathbf{A}\mathbf{C}_{\mathbf{yh}} + \mathbf{C}_{\mathbf{h}} \right\} \ ,
\end{aligned} \tag{A.8}$$

with the auto covariance matrix $\mathbf{C}_{\mathbf{h}} = \mathbb{E}\{\mathbf{h}\mathbf{h}^H\}$ and the cross covariance matrix $\mathbf{C}_{\mathbf{hy}} = \mathbb{E}\{\mathbf{h}\mathbf{y}^H\}$ where $\mathbf{h}$ and $\mathbf{z}$ have zero mean, i.e., $\mathbb{E}\{\mathbf{h}\} = 0$ and $\mathbb{E}\{\mathbf{z}\} = 0$. This minimization problem can be solved by

$$\begin{aligned}
\partial_{\mathbf{A}} \left\{ \mathbf{A}\mathbf{C}_{\mathbf{y}}\mathbf{A}^H - \mathbf{C}_{\mathbf{hy}}\mathbf{A}^H - \mathbf{A}\mathbf{C}_{\mathbf{yh}} + \mathbf{C}_{\mathbf{h}} \right\} &= 0 \\
\mathbf{C}_{\mathbf{y}}\mathbf{A}^H - \mathbf{C}_{\mathbf{yh}} &= 0 \ ,
\end{aligned} \tag{A.9}$$

finally yielding

$$\mathbf{A}^{\mathrm{LMMSE}} = \mathbf{C}_{\mathbf{hy}}\mathbf{C}_{\mathbf{y}}^{-1} \ . \tag{A.10}$$

A.3 The Least-Norm Solution for Underdetermined Problems

In general the minimization problem

$$\hat{\mathbf{h}} = \arg\min_{\mathbf{h}} \left\| \mathbf{y} - \mathbf{R}\mathbf{h} \right\|_2^2 \ . \tag{A.11}$$

with $\mathbf{R} \in \mathbb{R}^{m \times n}$ and $n > m$ has no unique solution. Choosing the least-norm solution for $\mathbf{h}$ is equivalent to minimizing

$$\begin{aligned}
&\underset{\mathbf{h}}{\text{minimize}} && \|\mathbf{h}\|_2^2 \\
&\text{subject to} && \mathbf{y} = \mathbf{R}\mathbf{h}
\end{aligned} \tag{A.12}$$

which can solved by introducing Lagrange multiplier $\boldsymbol{\lambda} \in \mathbb{R}^{m \times 1}$ [36], yielding

$$L(\mathbf{h}, \boldsymbol{\lambda}) = \mathbf{h}^H\mathbf{h} + \boldsymbol{\lambda}^H(\mathbf{R}\mathbf{h} - \mathbf{y}) \ . \tag{A.13}$$

The minimization is therefore solved by

$$\partial_{\mathbf{h}} L(\mathbf{h}, \boldsymbol{\lambda}) = \mathbf{R}\mathbf{h} - \mathbf{y} = 0 \ , \tag{A.14a}$$

$$\partial_{\boldsymbol{\lambda}} L(\mathbf{h}, \boldsymbol{\lambda}) = 2\mathbf{h}^H + \boldsymbol{\lambda}^H \mathbf{R} = 0 \ . \tag{A.14b}$$

Substituting (A.14b) into (A.14a) yields $\mathbf{y} = -\frac{1}{2}\mathbf{R}\mathbf{R}^H\boldsymbol{\lambda}$. Inserting this into (A.14b) finally yields the least-norm solution

$$\hat{\mathbf{h}}^{\mathrm{LN}} = \mathbf{R}^H \left(\mathbf{R}\mathbf{R}^H\right)^{-1} \mathbf{y} \ . \tag{A.15}$$

A.4 The Least Squares Solution for Overdetermined Problems

The overdetermined LS minimization problem

$$\begin{aligned} \hat{\mathbf{h}}^{\mathrm{LS}} &= \arg\min_{\mathbf{h}} \left\| \mathbf{y} - \mathbf{R}\mathbf{h} \right\|_2^2 \\ &= \arg\min_{\mathbf{h}} \left(\mathbf{y} - \mathbf{R}\mathbf{h}\right)^H \left(\mathbf{y} - \mathbf{R}\mathbf{h}\right) \ , \end{aligned} \tag{A.16}$$

with $\mathbf{R} \in \mathbb{C}^{m \times n}$ and $m \geq n$ is solved by

$$\begin{aligned} \partial_{\mathbf{h}} \left\{ \left(\mathbf{y} - \mathbf{R}\mathbf{h}\right)^H \left(\mathbf{y} - \mathbf{R}\mathbf{h}\right) \right\} &= 0 \\ -\mathbf{y}^H\mathbf{R} + \mathbf{h}^H\mathbf{R}^H\mathbf{R} &= 0 \ . \end{aligned} \tag{A.17}$$

This leads to the solution

$$\hat{\mathbf{h}}^{\mathrm{LS}} = \left(\mathbf{R}^H\mathbf{R}\right)^{-1} \mathbf{R}^H\mathbf{y} \ . \tag{A.18}$$

A.5 Sliding Averaging

The sliding averaging estimation method is given by (5.37). For the purpose of readability, this equation is limited to values of k for which the averaging window is not limited by the lower and upper boarder of the transmission band. A full channel estimated for all subcarriers $k \in \{1, \ldots, N_{\mathrm{SC}}\}$ is obtained by

$$\hat{\mathbf{h}}_{i,l}^{\mathrm{SAV}}[k] = \frac{1}{\bar{\gamma}\beta} \sum_{t=(k-\bar{\gamma})^+ + 1}^{k-(k-(N_{\mathrm{SC}}-\bar{\gamma}+1))^+} \ \sum_{j=t}^{t+\bar{\gamma}-1} \tilde{\mathbf{h}}_{i,l}[j] \tag{A.19}$$

with the number of elements in the first sum given by $\beta = k - (k - (N_{\mathrm{SC}} - \bar{\gamma} - (k - \bar{\gamma})^+$. Here the function $(\cdot)^+$ yields only the positive values of the argument, as

$$(x)^+ = \begin{cases} x & \text{for } x \geq 0 \\ 0 & \text{for } x < 0 \end{cases} \ . \tag{A.20}$$

A.6 The Quadratic Smoothing Estimator

The QS minimization problem

$$\begin{aligned}\hat{\mathbf{h}}^{\mathrm{QS}} &= \arg\min_{\mathbf{h}} \left\|\mathbf{y}-\mathbf{R}\mathbf{h}\right\|_2^2 + \lambda\left\|\mathbf{Q}\mathbf{h}\right\|_2^2 \\ &= \arg\min_{\mathbf{h}} \left(\mathbf{y}-\mathbf{R}\mathbf{h}\right)^H\left(\mathbf{y}-\mathbf{R}\mathbf{h}\right) - \lambda\left(\mathbf{Q}\mathbf{h}\right)^H\left(\mathbf{Q}\mathbf{h}\right) \ , \end{aligned} \tag{A.21}$$

is solved by

$$\begin{aligned}\partial_{\mathbf{h}}\left\{\left(\mathbf{y}-\mathbf{R}\mathbf{h}\right)^H\left(\mathbf{y}-\mathbf{R}\mathbf{h}\right) - \lambda\left(\mathbf{Q}\mathbf{h}\right)^H\left(\mathbf{Q}\mathbf{h}\right)\right\} &= 0 \\ -\mathbf{y}^H\mathbf{R} + \mathbf{h}^H\mathbf{R}^H\mathbf{R} + \lambda\mathbf{h}^H\mathbf{Q}^H\mathbf{Q} &= 0 \ . \end{aligned} \tag{A.22}$$

This leads to the solution

$$\hat{\mathbf{h}}^{\mathrm{QS}} = \left(\mathbf{I}_{N_{\mathrm{SC}}} + \lambda\mathbf{Q}^H\mathbf{Q}\right)^{-1}\mathbf{R}^H\mathbf{y} \ . \tag{A.23}$$

A.7 Inverse of a tri-diagonal Toeplitz Matrix

The inverse of the tridiagonal Toeplitz matrix

$$\mathbf{A} = \begin{pmatrix} a & b & & & \\ c & a & b & & \\ & \ddots & \ddots & \ddots & \\ & & c & a & b \\ & & & c & a \end{pmatrix} \in \mathbb{R}^{N\times N} \tag{A.24}$$

is explicitly known [41] to be

$$\mathbf{A}^{-1}[i,j] = \begin{cases} (-1)^{i+j}\frac{b^{j-i}}{\left(\sqrt{bc}\right)^{j-i+1}}\frac{U_{i-1}(d)U_{N-j}(d)}{U_N(d)} & \text{for } i \le j \ , \\ (-1)^{i+j}\frac{c^{i-j}}{\left(\sqrt{bc}\right)^{i-j+1}}\frac{U_{j-1}(d)U_{N-i}(d)}{U_N(d)} & \text{for } i > j \ , \end{cases} \tag{A.25}$$

with $d = a/(2\sqrt{bc})$ and $U_n(x)$ being the Chebyshev[15] polynomials of second kind and order n.

[15] Please note, that there are many different versions of this name commonly in use.

A.8 Mean Square Error Calculation

As an simulation metric, the empirical CE MSE is calculated as the average MSE over all scheduled subcarriers $k = \{1, \ldots, N_{\mathrm{SC}}\}$ and OFDM symbol times $n = \{1, \ldots, 14\}$ for all effective MIMO channels from active spatial layer $l = \{1, \ldots, N_L\}$ to receive antenna $i = \{1, \ldots, N_R\}$. Therefore the MSE is obtained by

$$\mathrm{MSE} = \frac{1}{N_R N_L 14 N_{\mathrm{SC}}} \sum_{i=1}^{N_R} \sum_{l=1}^{N_L} \sum_{n=1}^{14} \sum_{k=1}^{N_{\mathrm{SC}}} \left| \mathbf{h}_{n,i,l}[k] - \hat{\mathbf{h}}_{n,i,l}[k] \right|^2 , \tag{A.26}$$

with the actual channel $\mathbf{h}$ and the estimated channel $\hat{\mathbf{h}}$. In case of MU-MIMO transmission, spatial layers l have to be substituted by users $u \in \{1, \ldots, N_u\}$.

List of Figures

List of Tables

References

[1] Erich Zöchmann, Stefan Schwarz, Sefan Pratschner, Lukas Nagel, Martin Lerch, and Markus Rupp. "Exploring the Physical Layer Frontiers of Cellular Uplink - The Vienna LTE-A Simulator". In: *Eurasip Journal on Wireless Communications and Networking* (2016).

[2] Stefan Pratschner and Erich Zöchmann. "LTE-Advanced Uplink Transmissions". In: *The Vienna LTE-Advanced Simulators*. Springer, 2016, pp. 177–201.

[3] Stefan Pratschner, Erich Zöchmann, and Markus Rupp. "Low complexity estimation of frequency selective channels for the LTE-A uplink". In: *IEEE Wireless Communications Letters* 4.6 (2015), pp. 673–676.

[4] Lukas Nagel, Stefan Pratschner, Stefan Schwarz, and Markus Rupp. "Efficient Multi-User MIMO Transmissions in the LTE-A Uplink". In: *International Workshop on Link- and System Level Simulations (IWSLSS)*. Vienna, July 2016. In press.

[5] 3rd Generation Partnership Project (3GPP). *Requirements for further advancements for Evolved Universal Terrestrial Radio Access (E-UTRA) (LTE-Advanced)*. TR 36.913. 3rd Generation Partnership Project (3GPP), Dec. 2015.

[6] Sinem Coleri, Mustafa Ergen, Anuj Puri, and Ahmad Bahai. "Channel estimation techniques based on pilot arrangement in OFDM systems". In: *IEEE Transactions on Broadcasting* 48.3 (2002), pp. 223–229.

[7] Qi Jiang, Joachim Speidel, and Chunming Zhao. "Pilot-assisted OFDM channel estimation and ICI cancellation for double selective channels". In: *IEEE Global Telecommunications Conference (GLOBECOM'07)*. 2007, pp. 4150–4154.

[8] Yang Qin, Bing Hui, and KyungHi Chang. "Performance and complexity evaluation of pilot-based channel estimation algorithms for 3GPP LTE downlink". In: *IEEE Second International Conference on Ubiquitous and Future Networks (ICUFN)*. 2010, pp. 218–221.

[9] Ömer Çetin, Bahattin Karakaya, and Hakan Ali Cırpan. "Low complexity channel estimation for 3GPP LTE downlink MIMO OFDM systems". In: *IEEE 7th International Wireless Communications and Mobile Computing Conference (IWCMC)*. 2011, pp. 1441–1444.

[10] 3rd Generation Partnership Project (3GPP). *Evolved Universal Terrestrial Radio Access (E-UTRA) physical channels and modulation*. TS 36.211. 3rd Generation Partnership Project (3GPP), Jan. 2015.

[11] Xiaolin Hou, Zhan Zhang, and H. Kayama. "DMRS Design and Channel Estimation for LTE-Advanced MIMO Uplink". In: *IEEE 70th Vehicular Technology Conference Fall (VTC 2009-Fall)*. Sept. 2009, pp. 1–5.

[12] Edward Kasem and Jan Prokopec. "The evolution of LTE to LTE-Advanced and the corresponding changes in the uplink reference signals". In: *Elektrorecvue, ISSN* (2012), pp. 1213–1539.

[13] Meilong Jiang, Guosen Yue, Narayan Prasad, and Sampath Rangarajan. "Enhanced DFT-based channel estimation for LTE uplink". In: *IEEE 75th Vehicular Technology Conference (VTC Spring)*. 2012, pp. 1–5.

[14] Gillian Huang, Andrew Nix, and Simon Armour. "DFT-based channel estimation and noise variance estimation techniques for single-carrier FDMA". In: *IEEE 72nd Vehicular Technology Conference Fall (VTC 2010-Fall)*. 2010, pp. 1–5.

[15] Qingchuan Zhang, Xudong Zhu, Tao Yang, and Jin Liu. "An Enhanced DFT-Based Channel Estimator for LTE-A Uplink". In: *IEEE Transactions on Vehicular Technology* 62.9 (Nov. 2013), pp. 4690–4696.

[16] Meili Zhou, Bin Jiang, Wen Zhong, and Xiqi Gao. "Efficient channel estimation for LTE uplink". In: *IEEE International Conference on Wireless Communications & Signal Processing (WCSP)*. 2009, pp. 1–5.

[17] H. Sahlin and A Persson. "Aspects of MIMO Channel Estimation for LTE Uplink". In: *IEEE Vehicular Technology Conference (VTC Fall)*. Sept. 2011, pp. 1–5.

[18] Y Kang, K Kim, and H Park. "Efficient DFT-based channel estimation for OFDM systems on multipath channels". In: *IET Communications* 1.2 (2007), pp. 197–202.

[19] Edward Kasem, Roman Marsalek, and Jiri Blumenstein. "Performance of LTE Advanced Uplink in a Flat Rayleigh Channel". In: *Advances in Electrical and Electronic Engineering* 11.4 (2013), p. 266.

[20] Meili Zhou, Bin Jiang, Ting Li, Wen Zhong, and Xiqi Gao. "DCT-based channel estimation techniques for LTE uplink". In: *IEEE 20th International Symposium on Personal, Indoor and Mobile Radio Communications*. 2009, pp. 1034–1038.

[21] Fengwei Liu, Han Wei, Hongzhi Zhao, and Youxi Tang. "A novel channel estimation for MIMO SC-FDMA systems". In: *IEEE International Conference on Communications, Circuits and Systems (ICCCAS)*. Vol. 1. 2013, pp. 96–99.

[22] Zhijun Rong and Gerhard Fettweis. “Multi-user channel estimation for interference mitigation in the LTE-advanced uplink”. In: *IEEE 72nd Vehicular Technology Conference Fall (VTC 2010-Fall)*. 2010, pp. 1–5.

[23] Xingliang Zhang and Yabo Li. “Optimizing the MIMO Channel Estimation for LTE-Advanced Uplink”. In: *IEEE International Conference on Connected Vehicles and Expo (ICCVE)*. Dec. 2012, pp. 71–76.

[24] Qiang Li, Yuchun Wu, Shulan Feng, Peng Zhang, Lixia Xue, and Yongxing Zhou. “On Channel Estimation for Multi-User MIMO in LTE-A Uplink”. In: *IEEE 79th Vehicular Technology Conference (VTC Spring)*. 2014, pp. 1–5.

[25] Ravi Narasimhan and Shi Cheng. “Channel estimation and co-channel interference rejection for LTE-Advanced MIMO uplink”. In: *IEEE Wireless Communications and Networking Conference (WCNC)*. 2012, pp. 416–420.

[26] Chih-Ying Chen and D.W. Lin. “Channel estimation for LTE and LTE-A MU-MIMO uplink with a narrow transmission band”. In: *IEEE International Conference on Acoustics, Speech and Signal Processing (ICASSP)*. May 2014, pp. 6484–6488.

[27] Yang-Seok Choi, Peter J Voltz, and Frank A Cassara. “On channel estimation and detection for multicarrier signals in fast and selective Rayleigh fading channels”. In: *IEEE Transactions on Communications* 49.8 (2001), pp. 1375–1387.

[28] Michael Meidlinger, Michal Simko, Qi Wang, and Markus Rupp. “Channel estimators for LTE-A downlink fast fading channels”. In: *17th International ITG Workshop on Smart Antennas (WSA)*. VDE. 2013, pp. 1–5.

[29] R. Nissel and M. Rupp. “Doubly-selective MMSE channel estimation and ICI mitigation for OFDM systems”. In: *IEEE International Conference on Communications (ICC)*. June 2015, pp. 4692–4697.

[30] Erich Zöchmann, Stefan Pratschner, Stefan Schwarz, and Markus Rupp. “Limited feedback in OFDM systems for combating ISI/ICI caused by insufficient cyclic prefix length”. In: *Proc. IEEE Asilomar Conf. on Signals, Systems, and Comp.* Nov. 2014.

[31] A Wilzeck, Q Cai, M Schiewer, and T Kaiser. “Effect of multiple carrier frequency offsets in MIMO SC-FDMA systems”. In: *Proceedings of the International ITG/IEEE Workshop on Smart Antennas*. 2007.

[32] Erich Zöchmann, Stefan Pratschner, Stefan Schwarz, and Markus Rupp. "MIMO Transmission over High Delay Spread Channels with Reduced Cyclic Prefix Length". In: *Proceedings of 19th International ITG Workshop on Smart Antennas (WSA2015)*. VDE. 2015, pp. 1–8.

[33] Chester Sungchung Park, Y-P Eric Wang, George Jöngren, and David Hammarwall. "Evolution of uplink MIMO for LTE-advanced". In: *IEEE Communications Magazine* 2.49 (2011), pp. 112–121.

[34] Erik Dahlman, Stefan Parkvall, and Johan Sköld. *4G: LTE/LTE-advanced for mobile broadband*. Academic press, 2013.

[35] Markus Rupp, Stefan Schwarz, and Martin Taranetz. *The Vienna LTE-Advanced Simulators: Up and Downlink, Link and System Level Simulation*. Springer, 2016.

[36] Stephen Boyd and Lieven Vandenberghe. *Convex optimization*. Cambridge: Cambridge university press, 2009.

[37] R. Gribonval. "Should Penalized Least Squares Regression be Interpreted as Maximum A Posteriori Estimation?" In: *IEEE Transactions on Signal Processing* 59.5 (May 2011), pp. 2405–2410.

[38] 3rd Generation Partnership Project (3GPP). *Universal Mobile Telecommunications System (UMTS) Deployment aspects*. TR 25.943. 3rd Generation Partnership Project (3GPP), Feb. 2010.

[39] ITU. *Guidelines for Evaluation of Radio Transmission Technologies for IMT-2000*. Rec. M.1225. ITU, 1997.

[40] Bernard Sklar. "Rayleigh fading channels in mobile digital communication systems. I. Characterization". In: *IEEE Communications Magazine* 35.9 (1997), pp. 136–146.

[41] C.M. Da Fonseca and J. Petronilho. "Explicit inverse of a tridiagonal k-Toeplitz matrix". In: *Numerische Mathematik* 100.3 (2005), pp. 457–482.

[42] C. Mehlführer, J. C. Ikuno, M. Simko, S. Schwarz, and M. Rupp. "The Vienna LTE Simulators - Enabling Reproducibility in Wireless Communications Research". In: *EURASIP Journal on Advances in Signal Processing (JASP) special issue on Reproducible Research* (2011). doi:10.1186/1687-6180-2011-29.

[43] URL: `http://www.nt.tuwien.ac.at/ltesimulator/`.

[44] Hyundong Shin and Jae Hong Lee. "Capacity of multiple-antenna fading channels: spatial fading correlation, double scattering, and keyhole". In: *IEEE Transactions on Information Theory* 49.10 (2003), pp. 2636–2647.

[45] Yuyu Yan, Huiyu Yuan, Naizheng Zheng, and S. Peter. "Performance of uplink multi-user MIMO in LTE-advanced networks". In: *International Symposium on Wireless Communication Systems*. Aug. 2012, pp. 726–730.

[46] Rapeepat Ratasuk and Amitava Ghosh. "System Performance of Uplink Multi-User MIMO in LTE". In: *IEEE Vehicular Technology Conference (VTC Fall)*. 2011, pp. 1–5.

[47] Martin Lerch. "Experimental Comparison of Fast-Fading Channel Interpolation Methods for the LTE Uplink". In: *Proceedings of Elmar 2015*. Zadar, Croatia, Sept. 2015.

[48] Illia Safiulin, Stefan Schwarz, and Markus Rupp. "System level simulation of LTE MBSFN networks with high mobility users". In: *2015 International Conference on Systems, Signals and Image Processing (IWSSIP)*. IEEE. 2015, pp. 21–24.

[49] Alfio Quarteroni, Riccardo Sacco, and Fausto Saleri. *Numerical mathematics*. Vol. 37. Springer Science & Business Media, 2010.

[50] URL: `http://de.mathworks.com/help/matlab/ref/interp1.html`.

[51] Zijian Tang, Rocco Claudio Cannizzaro, Geert Leus, and Paolo Banelli. "Pilot-assisted time-varying channel estimation for OFDM systems". In: *IEEE Transactions on Signal Processing* 55.5 (2007), pp. 2226–2238.

[52] Thomas Zemen and Christoph F Mecklenbräuker. "Time-variant channel estimation using discrete prolate spheroidal sequences". In: *IEEE Transactions on Signal Processing* 53.9 (2005), pp. 3597–3607.

[53] David Slepian. "Prolate spheroidal wave functions, Fourier analysis, and uncertainty—V: The discrete case". In: *Bell System Technical Journal* 57.5 (1978), pp. 1371–1430.

[54] Xiaodai Dong, Wu-Sheng Lu, and Anthony CK Soong. "Linear interpolation in pilot symbol assisted channel estimation for OFDM". In: *IEEE Transactions on Wireless Communications* 6.5 (2007), pp. 1910–1920.

[55] Yahong Rosa Zheng and Chengshan Xiao. "Simulation models with correct statistical properties for Rayleigh fading channels". In: *IEEE Transactions on Communications* 51.6 (2003), pp. 920–928.

[56] Peter Hoeher, Stefan Kaiser, and Patrick Robertson. "Two-dimensional pilot-symbol-aided channel estimation by Wiener filtering". In: *IEEE International Conference on Acoustics, Speech, and Signal Processing (ICASSP-97)*. Vol. 3. 1997, pp. 1845–1848.

Hiermit erkläre ich, dass die vorliegende Arbeit gemäß dem Code of Conduct - Regeln zur Sicherung guter wissenschaftlicher Praxis (in der aktuellen Fassung des jeweiligen Mitteilungsblattes der TU Wien), insbesondere ohne unzulässige Hilfe Dritter und ohne Benutzung anderer als der angegebenen Hilfsmittel, angefertigt wurde. Die aus anderen Quellen direkt oder indirekt übernommenen Daten und Konzepte sind unter Angabe der Quelle gekennzeichnet.

Die Arbeit wurde bisher weder im In- noch im Ausland in gleicher oder in ähnlicher Form in anderen Prüfungsverfahren vorgelegt.

Wien, 20. Mai 2016

Stefan Pratschner, BSc